Isothermal evaporation of α-pinene secondary organic aerosol particles formed under low-NO_x and high-NO_x conditions

Zijun Li[1], Angela Buchholz[1], Luis M.F. Barreira[1,2], Arttu Ylisirniö[1], Liqing Hao[1], Iida Pullinen[1], Siegfried Schobesberger[1], Annele Virtanen[1,*]

[1]Department of Applied Physics, University of Eastern Finland, Kuopio, Finland

[2]Atmospheric Composition Research, Finnish Meteorological Institute, Helsinki, Finland

Correspondence to: Annele Virtanen (annele.virtanen@uef.fi)

Abstract. Many recent secondary organic aerosol (SOA) studies mainly focus on biogenic SOA particles formed under low-NO_x conditions and thus are applicable to pristine environments with minor anthropogenic influence. Although interactions between biogenic volatile organic compounds and NO_x are important in, for instance, suburban areas, there is still a lack of knowledge about volatility and processes controlling the evaporation of biogenic SOA particles formed in the presence of high concentrations of NO_x. Here we provide detailed insights into the isothermal evaporation of α-pinene SOA particles that were formed under low-NO_x and high-NO_x conditions to investigate the evaporation process and the evolution of particle composition during the evaporation in more detail. We coupled Filter Inlet for Gases and AEROsols-Chemical Ionization Mass Spectrometer (FIGAERO-CIMS) measurements of the molecular composition and volatility of the particle phase with isothermal evaporation experiments conducted under a range of relative humidity (RH) conditions from ~~dry~~ low RH (< 7 % RH) to high RH (80 % RH). Very similar changes were observed in particle volatility at any set RH during isothermal evaporation for the α-pinene SOA particles formed under low-NO_x and high-NO_x conditions. However, there were distinct differences in the initial composition of the two SOA types, possibly due to the influence of NO_x on the RO_2 chemistry during SOA formation. Such compositional differences consequently impacted the primary type of aqueous-phase processes in each type of SOA particles in the presence of particulate water.

1 Introduction

Biogenic secondary organic aerosol (SOA) affects the climate by scattering solar radiation (Lihavainen et al., 2015) and acting as cloud condensation nucleic (Sporre et al., 2014; Yli-Juuti et al., 2021). It overall causes a negative radiative forcing on climate and potentially offsets approximately 13 % of the warming effect due to a doubling of CO_2 (Sporre et al., 2019). Nonetheless, due to its short atmospheric lifetime (i.e., days to weeks) (Hodzic et al., 2016), biogenic SOA cannot be simply regarded as a long-term offset to the warming impact from the long-lived CO_2 (i.e., lifetime of years) (Myhre et al., 2013). Accurate assessments of the radiative forcing from biogenic SOA require a comprehensive understanding about the key processes affecting its atmospheric lifetime. As one of those processes controlling aerosol lifetime, evaporation governs the gas-particle partitioning of organic compounds. The recent findings of evaporation studies are primarily applicable to pristine forest areas (Vaden et al., 2011; Yli-Juuti et al., 2017; Buchholz et al., 2019; Li et al., 2019; Li et al., 2021), hence there is still a lack of information about the evaporation behavior of biogenic SOA particles in polluted areas where anthropogenic–biogenic interactions are important. Here, we investigate the isothermal evaporation of biogenic SOA particles which are derived from oxidizing one representative biogenic compound (BVOC) precursor in the presence of nitrogen oxides ($NO_x \equiv NO+NO_2$) that are important gaseous pollutants. The results of this study will help redefine the atmospheric lifetime of biogenic

SOA in, for instance, suburban areas that have experienced rapid growth of CO_2 emissions in the recent decade (Mitchell et al., 2018).

BVOCs account for up to 90 % of the global budget of non-methane volatile organic compounds (Guenther et al., 1995). Atmospheric oxidation of BVOCs produces condensable vapors and subsequently contributes to the formation of biogenic SOA (Ehn et al., 2014; Jokinen et al., 2015). With annual emissions of approximately 157–177 Tg, monoterpenes ($C_{10}H_{16}$) have been considered as an important class of BVOCs (Guenther et al., 2012) and recognized as a significant source of biogenic SOA not only in boreal forest areas (Tunved et al., 2006; Mohr et al., 2019; Barreira et al., 2021) but also in certain isoprene-dominated regions (Zhang et al., 2018; Lee et al., 2020). As monoterpene with the highest emissions from terrestrial vegetation, α-pinene has been commonly used as a proxy for monoterpenes. Oxidizing α-pinene with ozone (O_3) or hydroxyl radicals (OH) produces SOA particles with high particle viscosities (Virtanen et al., 2010; Saukko et al., 2012) and substantial amounts of oxidation products of low volatility (Lopez-Hilfiker et al., 2015; Ylisirniö et al., 2020). Compared to semi-volatile organic mixtures, α-pinene SOA particles display slower evaporation rates, which are attributed to the existence of compounds of low volatility, high particle viscosity and possible particle-phase reactions (Vaden et al., 2011; Yli-Juuti et al., 2017; D'Ambro et al., 2018). While kinetic limitations arising from particle viscosity hinder particle evaporation especially under ~~dry~~ low-RH conditions, the volatility distributions of particulate constituents primarily control the particle evaporation rate at high relative humidity (RH). On the one hand, particulate water content acts a plasticizer accelerating the bulk-surface diffusion (Yli-Juuti et al., 2017; Li et al., 2019). On the other hand, it behaves as a catalyst to induce aqueous-phase processes which form organic compounds of low volatility especially for SOA particles with high ~~oxidization~~ oxidation levels (Buchholz et al., 2019; Li et al., 2021). All these findings primarily advance our knowledge about the evaporation processes of biogenic SOA particles but limited to those in remote forest areas lacking in anthropogenic influence.

Over the past few decades, increasing amounts of NO_x emissions have been released into the atmosphere due to rapid economic growth and urbanization (Duncan et al., 2016). In recent years, increasing attention has been paid to the chemical interactions between NO_x and BVOC emissions, especially monoterpenes in suburban areas. In the southern United States, increasing amounts of daytime NO_x were suggested to enhance the formation of monoterpene SOA and increase the likelihood of fragmentation chemistry that forms oxidation products with carbon number (C_{num}) smaller than 10 (Zhang et al., 2018). In the same location, the large nighttime production of monoterpene SOA was attributed to oxidation induced by NO_3 which is a product of NO_2 and O_3 (Xu et al., 2015). In the southwest Germany, NO_x accumulated at night drove the large production of multifunctional organic nitrates (ON) via the nocturnal chemistry between monoterpenes and NO_x, contributing up to 25 % in mass to the particulate organics (Huang et al., 2019). Furthermore, hydrolysis which converts ~~organic nitrates~~ON into HNO_3 has been suggested as an efficient sink for ~~organic nitrates~~ON in the particle phase (Zare et al., 2018; Zare et al., 2019). Depending on the alkyl substitutions, functional groups, and carbon backbones, the hydrolysis mechanism and rates can vary between different monoterpene-derived ~~organic nitrates~~ON (Wang et al., 2021). Overall, the addition of NO_x affects the formation of monoterpene SOA, the types of oxidation products, and potentially the properties of the resulted particles. For monoterpene SOA particles produced in the presence of NO_x, there is very limited knowledge about the evolution of particle properties during isothermal evaporation process.

In this study, we investigated the isothermal evaporation of SOA particles from oxidizing α-pinene under low-NO_x and high-NO_x conditions at room temperature with a wide range of RH. We examined the volume change as well as the evolution of the molecular composition of α-pinene SOA particles during isothermal evaporation. While most recent laboratory studies focusing on the evaporation process of biogenic SOA particles represent conditions relevant for pristine environments with minor anthropogenic influence, our work would be one of the few providing insights into the SOA evaporation under suburban settings involving anthropogenic-biogenic interactions.

2 Methods

2.1 Isothermal evaporation of SOA particles

An oxidation flow tube reactor (OFR) of 13.3 L was used to generate α-pinene SOA particles at ~ 40 RH % and 25 °C with a residence time of 160 seconds (Kang et al., 2007; Lambe et al., 2011). Experimental conditions and results of SOA generation are summarized in Table S1. The operation procedure of this OFR has been described previously (Buchholz et al., 2019; Li et al., 2021). Briefly, α-pinene was continuously injected into a heated flow of N_2 with a syringe pump (Kari et al., 2018) and then mixed with a humidified flow of N_2, O_2, O_3, and N_2O before entering into the OFR. Before being mixed with O_3, the mixing ratio of α-pinene was constantly monitored by a proton transfer reaction time-of-flight mass spectrometer (PTR-TOF 8000, Ionicon Analytik) using hydronium (H_3O^+) ions. Overall, 5 L min^{-1} of total flow containing α-pinene (250 – 300 ppb) and O_3 (~ 13 ppm) was introduced into the OFR for photooxidation. Inside the OFR, SOA was formed by oxidizing α-pinene by OH radicals, which were produced by photolyzing O_3 (~ 13 ppm) with 254-nm UV lamps in the presence of water vapor. In the high-NO_x case, ~~NO and NO_2 were produced in situ via the photolysis of~~ N_2O (99.5 % purity, mixing ratio inside OFR: 1.85 % in volume) were injected into the OFR for NO_x production. NO and NO_2 were produced via the reactions $N_2O + O(^1D) \rightarrow 2NO$ and $NO + O_3 \rightarrow NO_2 + O_2$ ~~with~~ under the illumination of the same 254-nm lamps inside the OFR (Lambe et al., 2017). For the two NO_x cases, the voltage of the 254-nm lamps was adjusted to ensure similar OH exposure. We used the KinSim model (Peng and Jimenez, 2019) and additionally implemented the reactions of RO_2 (Peng et al., 2019) for simulating the OFR chemistry. The OH exposure was estimated to be (1.82 ± 0.21) ~~(2.6 ± 0.3)~~ × ~~10^{11}~~ 10^{12} and (2.45 ± 0.09) ~~(1.72 ± 0.07)~~× ~~10^{11}~~ 10^{12} ~~molec cm^{-3}~~ molecules cm^{-3} s for low-NO_x and high-NO_x conditions. ~~after considering the external OH reactivity (Peng et al., 2015; Peng et al., 2016).~~ Under low-NO_x condition, OH and O_3 contributed to 96% and 4% of the loss of α-pinene. Under high-NO_x condition, NO_3 radicals were produced from the $NO_2+O_3 \rightarrow NO_3+ O_2$ reaction and also contribute to the oxidation of α-pinene. The fractional loss of α-pinene to OH, O_3 and NO_3 were 50%, 1% and 49%. For the high-NO_x case, the estimated ratio between the $[RO_2]$ + $[NO]$ and $[RO_2]$ + $[HO_2]$ pathways ($\frac{[RO_2]+[NO]}{[RO_2]+[HO_2]}$) was ~~1.30 ± 0.18~~0.84 ± 0.19. For each experiment under one NO_x condition, similar aerosol mass concentration in the OFR was ensured. Assuming a particle density of 1.5 g cm^{-3} which was estimated on the basis of the elemental ratios of molecular compositions in aerosol particles (Kuwata et al., 2012), the mass concentrations of polydisperse α-pinene SOA were 442 ± 30 and 139 ± 29 μg ~~e~~m^{-3} under low-NO_x and high-NO_x conditions, respectively. Between experiments, the OFR was flushed with purified air overnight with the same RH and illumination as the following experiment but without adding α-pinene and N_2O. Afterwards, the background particle number and the VOC mixing ratio were reduced to be below 2000 # cm^{-3} (mass concertation < 0.1 μg ~~e~~m^{-3}) and under the instrument limit of detection, respectively. Despite the careful cleaning procedure, we cannot exclude a small contamination of the system with N_2O (e.g., in tubing before the OFR) and/or HONO (a by-product of the in-situ NO_x production from N_2O) which may lead to a small production of NO_x in experiment where no N_2O was added ($[NO_x]$ < 8 ppb at the outlet of OFR). Hence, we labeled the experiments with no N_2O addition as "low-NO_x" and expect a very small contribution of NO_x-related compounds.

After the OFR, 2 L min^{-1} of the generated α-pinene SOA was passed through an ozone denuder coated with potassium iodide, and then size selected with two parallel nanometer aerosol differential mobility analyzers (NanoDMA, model 3085, TSI) operated in an open-loop setting with a sample-to-sheath flow ratio of 1:8 or 1:10. During the size selection, the gas ~~vapors~~ phase compounds were diluted by at least 2 orders of magnitude so that particle evaporation was initiated (Li and Chen, 2005). By varying the ratio of dry and humidified flows for the sheath flow of the NanoDMAs, the RH of particle samples was set to one of three desired conditions: ~~dry~~ low RH (< 7 %), intermediate RH (40 % RH), or high RH (80 % RH). Afterwards, the size-selected SOA particles with 80-nm electrical mobility diameters were fed into either bypass lines with varying length or stainless-steel residence time chambers (RTC) with volumes of 25 L or 100 L for isothermal evaporation, allowing residence

times (t_R) from seconds to hours. The vapor wall losses in the RTC were sufficiently fast with a vapor wall loss coefficient greater than 10^{-2} s^{-1}, ensuring negligibly low concentrations of gas ~~vapors~~ phase compounds in the RTC (Yli-Juuti et al., 2017). After each isothermal evaporation experiment, the NanoDMAs, bypass lines and RTCs were flushed for at least 12 h with purified air under the same RH condition as the following experiment.

2.2 Physical and chemical characterization of SOA particles

2.2.1 SMPS analysis

Particle size changes due to isothermal evaporation were periodically measured with a scanning mobility particle sizer (SMPS, TSI classifier model 3080, CPC 3775). We quantified the extent of particle isothermal evaporation using the volume fraction remaining (VFR) under the assumption of particle sphericity. Independent of changes in particle number or mass concentration, the VFR was determined as $(D_{p,t}/D_{p,0})^3$, where $D_{p,t}$ and $D_{p,0}$ are the measured size after residence time t of isothermal evaporation and the selected sizes at the start of isothermal evaporation, respectively. The selected size $D_{p,0}$ was calibrated against ammonium sulfate particles under the experimental RH conditions.

2.2.2 HR-ToF-AMS analysis

Elemental composition measurements of particle samples were conducted using a high-resolution time-of-flight aerosol spectrometer (HR-ToF-AMS, Aerodyne Research Inc.). The oxidation state (OS_c = 2 O:C – H:C) of particle samples was calculated with the improved ambient parameterizations (Canagaratna et al., 2015). Following the Eqs. (1) – (2) presented in Kiendler-Scharr et al. (2016), we estimated the mass concentration of ~~organic nitrate~~ON moieties on the basis of the ratio of NO_2^+ and NO^+. The values of NO_2^+/NO^+ for ammonium nitrate (i.e., from the ionization-efficiency calibration) and ~~organic nitrates~~ON were correspondingly set to 0.51 and 0.1. We also estimated the upper bound of ~~organic nitrates~~ON by assuming all observed nitrates are in the organic form. When sampling from the RTC during evaporation, particle mass concentration was not sufficient to derive reliable elemental composition values from the AMS measurements. Thus, we only presented the elemental composition data from particle samples right after size selection which experienced the least amount of particle evaporation.

2.2.3 FIGAERO-CIMS analysis

Composition and volatility of particle samples were characterized with a custom-built Filter Inlet for Gases and AEROsols (FIGAERO) (Ylisirniö et al., 2021) in combination with a high-resolution time-of-flight chemical ionization mass spectrometer (CIMS, Aerodyne Research Inc.) using the iodide ionization scheme (Lopez-Hilfiker et al., 2014). The operation of FIGAERO-CIMS has been detailed in previous studies (Lopez-Hilfiker et al., 2014; Ylisirniö et al., 2021). The FIGAERO inlet allows sequential gas and particle measurements using two individual inlets leading to the CIMS. Since we were interested in the changes in particle composition and volatility, the system was only deployed for measuring particle-phase compounds. The mass resolution of CIMS was between 4000 and 5000 and the ion molecule reaction chamber was actively controlled at a pressure of 100 mbar. Due to the lack of a reliable sensitivity and transmission calibration for the relevant compounds detected with FIGAERO-CIMS, ion signals are presented in counts per second (ct s^{-1}), i.e., variabilities in sensitivity and transmission between compounds were not accounted for.

During sample collection, particles were sampled either after size selection (i.e., fresh stages with avg. t_R = 0.25 h) or after isothermal evaporation in the RTC (i.e., RTC stages with avg. t_R = 4.25 h) onto a PTFE filter (2 µm pore, Zefluor, Pall Corp.) for 0.5 h. The collected particles were thermally desorbed from the filter into the CIMS using a temperature-controlled dry N_2 flow. The temperature of the N_2 flow was linearly increased from 25 °C to ~ 200 °C within 20 min (i.e., desorption period)

and then kept at ~200 °C for an extra 15 min (i.e., soak period) so that organic residuals, if any, could evaporate from the filter. Apart from particle samples, we also performed two different types of blank measurements to identify instrument background and potential contaminations from the sampling process. The instrument background was investigated by measuring clean FIGAERO filters with no particle collection, while additional contaminations were determined by analyzing samples which were collected through the NanoDMAs with a set voltage of 0 V (i.e., no selected particles) and 0.5-h collection time.

For each observed ion, the change in signal intensity with desorption temperature (T_{desorp}) is called thermogram. The desorption temperature with the maximum signal (T_{max}) is proportional to the saturation vapor concentration (C^*, defined at 25 °C) of a compound (Lopez-Hilfiker et al., 2014). In this study, the $T_{max} - C^*$ relationship was calibrated using a homologous series of polyethylene glycol compounds (PEG 4 - 8) as reference compounds (Ylisirniö et al., 2021). According to the volatility classification defined by Donahue et al. (2012), the range of T_{desorp} was divided into semi-volatile organic compounds (SVOCs), low-volatility organic compounds (LVOCs) and extremely low volatility organic compounds (ELVOCs). Note that the conducted calibration is sufficient to reliably identify the SVOC and LVOC ranges, despite uncertainties in extrapolating the calibration towards lower C^* values (Hyttinen et al., 2022). The measured calibration parameters are listed in the Supplement.

2.2.4 Positive matrix factorization analysis

Positive matrix factorization (PMF) (Paatero and Tapper, 1994) was deployed to analyze the mass spectra data collected by the FIGAERO-CIMS (Buchholz et al., 2020; Li et al., 2021). Organic compounds which have similar temporal behavior (i.e., similar thermal desorption behavior and/or aqueous phase process) during isothermal evaporation were grouped into a single factor. Blank samples were also included in the data sets for PMF analysis to determine background factors. Error matrices were prepared using the constant error scheme (Buchholz et al., 2020) without any down-weighting, and the PMF results were evaluated with the PMF Evaluation Tool (PET v3.05) (Ulbrich et al., 2009). Due to the predominance of non-nitrated ~~organics~~ organic compounds (labeled as "CHO compounds") in all particle samples (Table 1), the PMF analysis was independently applied to ~~non-nitrated organics~~ CHO compounds and ~~organic nitrates~~ON (labeled as "ON") so that the ~~organic nitrates~~ON could be better resolved into factors. This approach also allowed us to investigate potential similarities between the low-NO_x and high-NO_x experiments regarding the ~~non-nitrated organic~~CHO compounds. After careful comparisons between multiple PMF solutions, we decided to select PMF solutions with 12 and 8 factors for the dataset ~~non-nitrated organics~~CHO compounds and ~~organic nitrates~~the one of ON~~ data sets~~, respectively. We assigned each PMF factor as a sample or background factor according to its contribution in the particle and filter blank samples. For the ~~non-nitrated organics~~ data set of CHO compounds, 5 sample and 7 background factors were found. For the ~~organic nitrate~~ON data set, 3 out of the 8 factors were identified as sample factors. In the following discussion, only the sample factors will be considered, but the factor thermograms and mass spectra of all factors are shown in the Supplement. Note that the seemingly large number of background factors is due to changes in the exact composition of the instrument background between different experiment days (e.g., due to changing the PTFE filter in the FIGAERO inlet), i.e., each sample has contributions from only 2 or 3 out of all background factors. Detailed information on the PMF solution diagnostics can be found in the Supplement.

3 Results and Discussion

3.1 Isothermal evaporation and thermal desorption behavior of SOA particles

Changes in the VFR of particles as a function of t_R at different RH are presented for low-NOx (grey) and high-NOx (orange) conditions in Figure 1. The particle evaporation rates were almost identical between the two NOx conditions at any set RH. We acknowledge that certain amounts of inorganic nitrates (e.g., NH4NO3, HNO3) were formed under high-NOx conditions due to the high levels of gaseous HNO3 and HONO which were byproducts of the NO production via ~~N2O photolysis~~the

reaction between N2O and O(1D) (Lambe et al., 2017). However, estimated from the AMS data, the produced inorganic nitrates contributed approximately 1 % to the particle mass (Table 1) and would only lead to very minor changes in particle volume during isothermal evaporation (i.e., smaller than the measurement uncertainty). For comparing VFR values between studies, it is important to take particle composition into account (i.e., precursor compounds and oxidation level). The observed evaporation behavior fell between the medium- and high-O:C cases reported in Buchholz et al., 2019 (see Figure S1 in the Supplement), as expected from the measured O:C levels in this study.

With increasing RH, the particle evaporation rate became faster (Figure 1), and a larger fraction of compounds was removed during isothermal evaporation. As previous particle evaporation studies have suggested (Vaden et al., 2011; Yli-Juuti et al., 2017; Buchholz et al., 2019; Li et al., 2019; Zaveri et al., 2020; Li et al., 2021), considerable kinetic limitations exist in ~~dry~~ SOA particles at low RH and thus evaporation of compounds is slowed down due to the substantially high particle viscosity. With increasing RH, particulate water acts as a plasticizer for the bulk – surface diffusion and therefore enhances particle evaporation. In addition, the almost identical particle evaporation rates between intermediate-RH (40 % RH, diamonds) and high-RH (80 % RH, circles) conditions suggest that the particle evaporation at 40 % RH can be already approximated as a liquid-like process (Figure 1). ~~For the investigated SOA particles, we observed that particulate water also acted as a catalyzer for aqueous-phase processes (see section 3.4). Note that decoupling the plasticization and catalytic roles of particulate water on the SOA particle evaporation requires the development of process-level models considering particle-phase chemistry and is thus beyond the scope of this work.~~

To investigate if particulate water acted also as a catalyzer for aqueous-phase processes for the low- and high-NO_x cases, we calculated the expected isothermal evaporation behavior based on the particle-phase volatility distribution from the PMF analysis of the FIGAERO measurements (see section 3.2) by using a liquid-like evaporation model (LLEVAP) (Lehtinen and Kulmala, 2003; Yli-Juuti et al., 2017), which assumes particle volatility as the only driver for particle size change during particle evaporation (see section S1.1 in Supplement). With this method, Tikkanen et al. (2020) could reproduce the observed isothermal evaporation under high-RH conditions for α-pinene SOA particles if no substantial aqueous-phase processes occurred, and particulate water acted primarily as a plasticizer. But in this study, we found a clear discrepancy between the observed isothermal evaporation and the LLEVAP simulations even when considering the interquartile range of the volatility distribution (see Figure S2 in the Supplement). The volatility distribution derived from the FIGAERO measurement was too far in the LVOC and ELVOC range, i.e., using this volatility distribution always underestimates the amount of isothermal evaporation. This behavior can be interpreted as a sign for aqueous-phase processes. Water acted as a catalyst for reactions creating products of higher volatility which then evaporate from the particle, thus leading to more isothermal evaporation than expected from the original volatility distribution. We discuss more details about the changes in the composition of the residual particles and possible reaction pathways in section 3.4.

In Figure 2, we show the thermal desorption profiles for the high-NO_x case at fresh and RTC evaporation stages under ~~dry~~ low-RH (Figure 2c, d) and high-RH (Figure 2a, b) conditions. Thermal desorption behavior of particle samples is usually illustrated with sum thermograms (STGs) in which the total sum of organic signals is plotted against T_{desorp} (Lopez-Hilfiker et al., 2015; D'Ambro et al., 2017). Note that the appearances of STGs are impacted by both the total number of molecules collected onto the filters and the underlying volatility distributions. To allow feasible comparisons between fresh and RTC samples at the same RH, all STGs were at first normalized to the total ion signals of each individual sample. Following the same procedure described by Li et al. (2021), we then scaled the normalized STGs of the RTC samples with the changes in the average VFR (VFR_{avg}) between fresh and RTC stages to account for the expected particle volume change due to isothermal evaporation. To enhance readability, we will hereafter call both – the normalized STGs for the fresh samples and the scaled normalized STGs of the RTC samples – "STG", since they are now directly comparable.

The difference between STGs of fresh and RTC samples (Figure 2a, b; indicated as gray-striped areas) became larger when particulate water was present. Overall, ~~organic nitrates~~ON accounted for up to 20 % of the total organic signals of FIGAERO samples under high-NO_x conditions, which broadly agrees with the values estimated from the AMS data under the same condition (Table 1). Since thermal losses of nitrate moieties from ~~organic nitrates~~ON during FIGAERO desorption are possible (Francisco and Krylowski, 2005), the estimated fraction of ~~organic nitrates~~ON here represents the lower bound. We also examine changes in the median desorption temperature values (T_{50}) for the total organics, ~~non-nitrated organics~~CHO compounds, and ~~organic nitrates~~ON between different samples, as shown in Figure 2e. On average, the ~~organic nitrates~~ ON were slightly more volatile and had lower values of T_{50}, as compared to the ~~non-nitrated organics~~CHO compounds. In line with the faster particle evaporation rate at high RH (Figure 1) and larger removal of volatile compounds (Figure 2a-d), changes in T_{50} were more noticeable in the high-RH samples than the ~~dry~~ low-RH ones for all compositional categories (Figure 2e). Very similar changes in STGs and T_{50} were observed in the low-NO_x case in the Supplement.

3.2 PMF of SOA particles

In the following sessions, we presented the independent PMF analysis results for the ~~non-nitrated organics~~CHO compounds and ~~organic nitrates~~ON. The integrated mass spectra showing the overall composition for each particle sample are presented in the Supplement.

3.2.1 Characterization of ~~non-nitrated organics~~CHO compounds

As shown in Figure 3, five sample factors (i.e., F1 – 5) were identified for ~~non-nitrated organics~~CHO compounds. Ratios between sample factors changed when NO_x was present during SOA formation in the OFR. Compared with ~~non-nitrated organic~~CHO factors in the high-NO_x samples, the ~~organic nitrates~~ON (in purple; sum of the sample factors of the ~~organic nitrates~~ON data set, see section 3.2.2) overall spanned a volatility range similar to F2 and F3. Note that small amounts of ~~organic nitrates~~ON were observed in the low-NO_x sample with a signal contribution of 2 % or less to the particle sample. This was probably caused by small contaminations of the OFR system with N_2O from the preceding high-NO_x experiments. All ~~non-nitrated organic~~CHO factors except F4 mainly consisted of compounds with a molecular weight (MW) of less than 250 Da and with C_{num} of 10 or less (Figure 4). For the factors F1 – 4, the factor volatility which is indicated by the T_{50} values (Table 2) exhibited stronger dependence on the signal-weighted MW rather than the signal-weighted OS_c . Moreover, contributions of compounds with C_{num} of 10 or more to the factor spectra become more important with increased values of T_{50}. Since the increase of oxygen and hydrogen atoms counterbalances the simultaneous extension of carbon backbones, OS_c does not reflect the effect of MW on the factor volatility in this case. Even though F5 is the least volatile sample factor, the range of MW and C_{num} of the compounds grouped into F5 was very similar to that of F2. The combination of high T_{50} and the dominance of compounds with C_{num} of 10 or less in F5 very likely suggests that these compounds are largely the products from the thermal decomposition of (extremely) low-volatility parent compounds during the FIGAERO desorption. During a FIGAERO desorption cycle, a thermally labile compound starts to decompose into smaller compounds at desorption temperatures that are above its threshold temperature of decomposition. When the desorption temperature increases, thermal decomposition is enhanced, and more signal is detected for the decomposition products. For F5 specifically, the position of its T_{50} depends on the balance between the increasing decomposition and the availability of the decomposing compounds. Thus, the T_{50} value only provides a general idea about the temperature range in which the thermal decomposition of the compounds grouped into the F5 occurs. The thermal decomposition very likely happens at temperatures below the (theoretical) desorption temperature of the parent compounds. Thus, we can only obtain an "apparent" volatility with the use of the T_{50} value of F5.

3.2.2 Characterization of ~~organic nitrates~~ON

We identified three sample factors (i.e., NF1 – 3) from ~~organic nitrates~~ON, as shown in Figure 5 and described in Table 2. While NF1 – 3 only occurred in the high-NO_x samples, an additional sample factor was found in the low-NO_x ones. The formation of this unique sample factor in the low-NO_x samples was possibly due to the very small amount of NO_x being formed in the low-NO_x experiments. Since the total contribution of the ~~organic nitrates~~ ON in the low-NO_x samples was no more than 2 %, we here only focus on the analysis of the high-NO_x samples of which up to 20 % of particle mass were attributed to ~~organic nitrates~~ ON (Table 1). Accounting for the nitrogen content of ~~organic nitrates~~ON, we calculated the OS_c (i.e., $OS_c = 2 \cdot \frac{O}{C} - \frac{H}{C} - 5 \cdot \frac{N}{C}$) of each nitrogen-containing compound under the assumption that all nitrogen existed in the form of alkyl nitrates (Priestley et al., 2021). While NF2 and 3 appeared under all conditions, the contribution of NF1 to particle samples became significant only in the high-RH samples (Figure 5a), suggesting that the formation pathway of NF1 was different from the other two ~~organic nitrate~~ ON factors'. All the mass spectra of NF1 – 3 were dominated by compounds with C_{num} of 10 or less, although noticeable amounts of compounds with C_{num} > 10 were observed in NF3 (Figure 5b), consistent with its overall high value of T_{desorp} suggesting the lowest volatility among the ~~organic nitrate~~ ON factors.

3.3 Effect of NO_x on the α-pinene SOA formation

The signal contributions of ~~non-nitrated organic~~CHO sample factors to the total sum of organics were compared between low-NO_x (in grey) and high-NO_x cases (in orange) in Figure 6a. Here, only the ~~dry~~ low-RH particle samples collected at the fresh stages were chosen for analysis, as they were subject to the least amount of isothermal evaporation during the FIGAERO sample collection. Substantially large differences in the signal contributions were observed for multiple sample factors. Under low-NO_x condition, F1, F2, and F5 were the three major factors. For the high-NO_x samples, F3 was the dominant factor followed by approximately equal contributions from the other factors. Small but noticeable differences in the factor contributions were observed for F4 between the two NO_x conditions. The observed difference in the factor mass contribution between the investigated particle samples could be induced by the enhancement/suppression of formation pathways for certain compounds (Kroll and Seinfeld, 2008) and/or the gas–particle equilibrium partitioning which follows Raoult's law (Donahue et al., 2006). ~~According to the partitioning theory (Pankow, 1994) for a system in equilibrium between gas and particle phase, the C^* of a sample factor k can be expressed as~~

~~$$C_k^* = OA \cdot \frac{G_k}{P_k}, \quad (1)$$~~

~~where OA is the organic particle mass concentration, which was determined from SMPS data, by assuming a particle density of 1.5 μg m^{-3}. G_k and P_k represent the mass concentrations of a sample factor k in gas and particle phase, respectively.~~

~~Rearranging Eq. (1), we can calculate the total mass concentration of a sample factor k in both gas and particle phase as follows~~

~~$$G_k + P_k = (OA + C_k^*) \cdot \frac{P_k}{OA} \quad (2)$$~~

~~The C^* value of a sample factor k can be estimated by converting its T_{50} value into C^* at 25 °C with a parametrization derived from the T_{max} – C^* calibration. $\frac{P_k}{OA}$ is the mass contribution of a sample factor k in the initial particles prior to isothermal evaporation. Here, we use the mass fraction of a sample factor k in the dry, fresh samples as the proxy of $\frac{P_k}{OA}$, since these particle samples experienced the minimum amount of isothermal evaporation.~~

The total mass concentration in gas and particle phase for each sample factor ($G_k + P_k$) (see section S1.3 in the Supplement for more details of the estimation)~~, derived using Eq. (2),~~ is shown in Figure 6b. Addition of NO_x during SOA formation inside the OFR decreased the production (i.e., the sum of gas and particle mass concentrations) of the compounds grouped into F1,

F2, and F5, and increased the production of ~~organic nitrates~~ON. Therefore, changes in their individual contributions to the high-NO_x sample were primarily caused by the effect of NO_x on the formation of the compounds in these factor groups. Furthermore, it should be noted that for F3 and F4, their individual productions were comparable between the low-NO_x and high-NO_x cases. Thus, in comparison with the low-NO_x sample, the enhanced contributions of F3 and F4 to the high-NO_x sample were most likely due to the decreased contributions of other factors in the particle phase.

Note that the total mass concentration estimated in Eq. (S2) was under the assumption of the gas – particle equilibrium during the timescale of the OFR. Since particles were always produced at 40 % RH where negligible kinetic limitation exists, equilibrium should be reached between gas and particle phase during the minutes of residence in the OFR (Li and Shiraiwa, 2019). Another caveat to the discussion above is the potential occurrence of particle-phase reactions during SOA formation inside the OFR. Many of these reactions can be acid-catalyzed. Note that HNO_3 is formed as a byproduct when using N_2O to generate NO_x in the OFR (Lambe et al., 2017). Due to the lack of direct gaseous HNO_3 measurement, we used the KinSim model to estimate the concentration of gaseous HNO_3 produced under high-NO_x condition in the OFR. The gaseous HNO_3 concertation was estimated to be 927 ppb. Based on the coefficient for partitioning of gaseous HNO_3 to SOA described by Ranney and Ziemann (2016), the estimated particulate nitrate (i.e., $[HNO_3]_{SOA} + [NO_3^-]_{SOA}$) concentration is 0.20 μg m^{-3} for the polydisperse SOA (139 ± 29 μg m^{-3}) that was formed under the high-NO_x condition in the OFR. With similar gaseous concertation of HNO_3 (~ 1 ppm), Ranney and Ziemann (2016) observed 7.5 μg m^{-3} particulate nitrate in the presence of 3000 μg m^{-3} dry SOA that was formed from n-pentadecane with OH radicals. They also found that under such condition, 40% of the cyclic hemiacetals in the SOA can undergo particle-phase dehydration within three hours, with a dehydration rate constant (k_d) of 0.25 h^{-1}. Note that the α-pinene SOA in our study are highly oxidized and thus exhibit much higher polarity than the n-pentadecane SOA. It is likely that the k_d for the hemiacetals in the α-pinene SOA in our study is several orders magnitude smaller than the value reported for the cyclic hemiacetals in the SOA (Ranney and Ziemann, 2016). ~~Ranney and Ziemann (2016) reported that gaseous HNO_3 (0.25 – 2.0 ppm) was able to catalyze the particle-phase hemiacetal dehydration for alkane oxidation products. However, this type of reaction would not be relevant with respect to the OFR residence time, due to the negligible amount of HNO_3 produced in the OFR and its very long reaction timescale of weeks.~~ For non-catalyzed reactions, their reaction rates depend on their own reaction rate constants as well as both gas vapor concentration and condensation rate (Peng and Jimenez, 2020). Since information on the kinetics of non-catalyzed reactions is still rare, their importance on the SOA formation in the OFR is difficult to estimate.

3.4 Evolution of PMF factors during isothermal evaporation

By coupling the sample factor contributions from the FIGAERO measurement with changes in VFR_{avg} retrieved from the SMPS measurements during isothermal evaporation, we are able to derive the net change ratio (NCR) to evaluate the net transformation (i.e., material loss vs. production) of individual sample factors during isothermal evaporation (Li et al., 2021). Each factor in each particle sample is compared to its reference case (i.e., its contribution in the ~~dry~~low-RH, fresh condition). If a low-volatility factor simply remains in the particle phase (i.e., no change) or the formation and removal processes are equal to each other (i.e., no net change), NCR is equal to 1. NCR values > 1 mean that the contribution of the factor increases due to an actual formation process. NCR values < 1 indicate that the contribution of the factor decreases either due to evaporation or because the compounds grouped into this factor were consumed in particle-phase reactions. To determine if evaporation is the likely cause for the change, we use the characteristic desorption temperature (characteristic T_{desorp}) of the factor which is the desorption temperature at which 25 %, 50 %, and 75 % of the factor thermogram signal is reached. This measure gives a deeper insight into the shape of the thermogram than just using T_{50} and is a better representation of the volatility range of a factor.

3.4.1 NCR of ~~non-nitrated organics~~CHO compounds

The changes in NCR were minor in the ~~dry~~ low-RH samples for most sample factors (Figure 7b), which is consistent with the small change in VFR (Figure 1), STGs (Figure 2a-d), and particle composition (Figure 3),. Only F1, the sample factor with the lowest characteristic T_{desorp} (Figure 7a), displayed a different trend between the low-NO_x and high-NO_x cases, with a decrease in the NCR in the low-NO_x sample but almost no change in the high-NO_x one (Figure 7b). The NCR of ~~- organic nitrates~~ ON (i.e., sum of NF1 – 3) decreased with isothermal evaporation under ~~dry~~ low-RH conditions. Loss due to evaporation seems to be unlikely as they spanned a volatility range from LVOCs to ELVOCs. It is possible that when ~~organic nitrates~~ ON were able to decompose into HNO_3 and ~~non-nitrated organic~~CHO products during isothermal evaporation, the remaining organics might still be retained in the ~~dry~~ low-RH particle samples due to high particle viscosity and possibly contributed to F1 in the high-NO_x sample.

When particulate water was present, i.e., under high-RH conditions, the evolution of NCR became more complex. F1 already showed a lower value of NCR at the fresh stage compared to the ~~dry~~ low-RH conditions, and it was no longer present in the particle after isothermal evaporation in the RTC (indicated by cross symbols in Figure 7b). As the volatility of F1 was high enough to allow significant evaporation within 4.25 h, its decreasing NCR can still be primarily caused by evaporation. Similar to the case of F1, F2 and F4 also showed lower values of NCR in the presence of water as compared to the ~~dry~~ low-RH conditions. Contrary to the ~~dry~~ low-RH conditions, a clear decreasing trend in NCR of these factors with decreasing VFR_{avg} was observed under high-RH conditions already at the fresh stage. Since little evaporation is expected for compounds in the volatility range of LVOCs and ELVOCs to which F2 and F4 were assigned (Li et al., 2019), there must be another mechanism (i.e., aqueous-phase processes) primarily driving the loss of these compounds at the fresh stage with a timescale in the order of minutes. With increasing evaporation time at high RH, the evolution pattern of the NCR for ~~each factor diverged~~either F2 or F4 differed between two SOA types. In the high-NO_x case, the NCR values of F2 and F4 further decreased with evaporation time, which suggests that the material loss mechanism continued as the dominant pathway controlling their evolution during isothermal evaporation. In the low-NO_x case, however, their NCR values showed an increasing trend during isothermal evaporation, indicating that the chemical production of the grouped compounds outweighed the loss pathway at this stage. Although the NCR trends of F2 were different between the low-NO_x and high-NO_x cases under high-RH conditions, the characteristic T_{desorp} increased in both cases (Figure 7a). Such an increase was interpreted as an indication for aqueous-phase chemistry in a previous study (Buchholz et al., 2020). This may indicate, that for both cases, the presence of particulate water was crucial, but the extent or speed of the transformation varied.

When investigating F3 at high RH, the change in its NCR was dependent on the NO_x condition during SOA formation. Already for the fresh stage at high RH, the NCR of F3 showed a pronounced increase and became much larger than 1 in the low-NO_x case. However, the NCR of F3 stayed more or less at 1 in the high-NO_x case. As F3 falls in the range of LVOCs and ELVOCs (similar to F2), only little evaporation is expected within the time span of that case (avg. t_R = 0.25 h) (Li et al., 2019). Consequently, there must be an efficient production pathway under the high-RH condition that contributes to compounds assigned to F3 already at the fresh stage. The corresponding thermograms (red in Fig. 3, 3rd row) are alike in the low-NO_x and high-NO_x cases, suggesting that this production had occurred in both samples, but was more dependent on particulate water in the low-NO_x sample than in the high-NO_x one. A small but noticeable decrease due to isothermal evaporation is expected for compounds within the range of LVOCs for the timescale of 4.5 h (Li et al., 2019). When the low-NO_x particles continued to evaporate at high RH, the NCR of F3 indeed decreased. Considering the change in its factor thermogram shape (Figure 3a) and the minor shift in its characteristic T_{desorp} (Figure 7a) in the low-NO_x case at high RH, it is very likely that the decrease in the NCR of F3 during isothermal evaporation was mostly driven by the evaporation of its volatile content with high C^*. In the

high-NO_x samples, on the other hand, the NCR of F3 barely changed with evaporation time, even under high RH. In this case, there must be a production pathway, which compensated for the material loss for F3 in the high-NO_x sample.

Unlike the ~~dry~~ low-RH conditions, F5 already showed noticeable changes in its NCR at the fresh stage under high-RH condition. Since little evaporation was expected for compounds in the ELVOC range in the time span of hours (Li et al., 2019), the observed changes in the NCR of F5 in either NO_x case would suggest the existence of aqueous-phase processes already at the fresh stage. Similar to F3, the evolution of F5 with increasing evaporation also varied between the two particle types at high RH. With a decreasing VFR_{avg} (i.e., increasing isothermal evaporation), F5 showed a decrease in its NCR in the low-NO_x samples but exhibited an increase in its NCR in the high-NO_x ones. Such different evolution trends of the NCR of F5 between the two NO_x levels at high RH indicate that the competition between production and loss reactions in the aqueous phase varied with the SOA formation conditions.

~~3.4.2 Possible aqueous-phase processes affecting NCR of non-nitrated organics~~

~~When compounds dissociate (here, mostly hydrolyze) into smaller molecules, the products of this process can either evaporate from or stay in the particle phase and possibly participate in further reactions with other molecules. Note that products that evaporate do not contribute anymore to any of the factors. Linking two or more molecules via chemical bonds (accretion reactions) produces larger compounds of lower volatility which are less likely to evaporate. These products can undergo further reactions with increasing isothermal evaporation time especially in the presence of water. Note that if they have sufficiently low volatility, newly formed compounds from aqueous phase processes will remain in the particle phase and contribute to other factors.~~

~~In the high NO_x samples, only decreasing or constant NCR values were observed for factors F2 – F5 at the fresh stage under high RH conditions. This suggests that the reactions consuming F2 and F4 are mostly hydrolysis type processes (i.e., creating products that do not remain in the particle phase). The formation pathways for products grouping into F3 and F5 are minor. This formation of more volatile compounds may increase the observed isothermal evaporation of the particles. In the low NO_x case, we observed factors with increasing NCR (F3 and F5) and with decreasing NCR (F2 and F4) when RH increased. It is likely that the particle phase reaction involving compounds in F2 and/or F4 result in low volatility products contributed to F3 and F5. Hence, accretion type reactions must be the dominant pathway for this SOA type. Products from such accretion reactions could have sufficiently low volatility and slow down the particle evaporation, possibly resulting in the slightly larger VFR_{avg} in the low NO_x case (Figure 7c). One possible type of accretion reaction could be the Baeyer – Villiger reaction of peroxides (e.g., peroxycarboxylic acid and hydroperoxide) (Lim and Turpin, 2015; Claflin et al., 2018) which are expected to be relatively more abundant for the low NO_x samples of which $RO_2 + HO_2$ reactions were favored during SOA formation, compared to the high NO_x samples (Ziemann and Atkinson, 2012; Peng and Jimenez, 2020). Note that $RO_2 + HO_2$ reactions can also lead to the production of carboxylic acids. Although we cannot rule out the occurrence of Fischer esterification requiring carboxylic acids, such reaction could not be observed even in extremely acidic particles for the relevant time scales of hours (Birdsall et al., 2013; Kristensen et al., 2014).~~

~~When particles continued to evaporate in the RTC under high RH conditions, there were again differences in the evolution of F2 – F5 for low NO_x and high NO_x conditions. While F2 and F4 displayed continuous decreases in NCR in the high NO_x samples, these two factors experienced increases in their NCR in the low NO_x ones. Very likely, hydrolysis and accretion were the underlying reactions for the high NO_x case, and those resulted products of sufficient low volatility possibly contributed to the constant and increasing NCR values of F3 and F5. For the high NO_x samples, the important role of accretion at the RTC stage but not at the fresh stage might indicate the timescale required for such reaction to be in the order of hours. Kinetic measurements have suggested that while the peroxy hemiacetal formation involving peroxides and carbonyls has a timescale~~

~~from 1 min to 2h , the formation of hemiacetal from reactions between alcohol and carbonyls is at least one order of magnitude slower (i.e., timescale of 10h) (Ziemann and Atkinson, 2012). Furthermore, the increasing NCR of F2 and F4 in the low NO_x case was driven by the net production of compounds. This was likely attributed to the decomposition of compounds with short lifetime (e.g., acylperoxy hemiacetals and peroxy hemiacetals), originally (i.e., at the fresh stage) grouped into F3 and F5 (Claflin et al., 2018).~~

3.4.~~3~~ 2 NCR of ~~organic nitrates~~ON

Already under ~~dry~~ low-RH conditions, decreasing values of NCR were observed for NF2 and NF3 after isothermal evaporation in the RTC. As some compounds grouped into NF2 desorbed in the SVOC range (Figure 5a~~-~~,1st and 2nd rows), loss due to evaporation is a possible explanation for the behavior of NF2. However, the volatility of NF3 was in the ELVOC range and so little evaporation is expected even under high RH (Li et al., 2019). Thus, the decreasing NCR for NF3 under ~~dry~~ low-RH conditions can possibly be attributed to the chemical decomposition of the ~~organic nitrates~~ON. When particles were conditioned to RH below 10 % in the ~~dry~~ low-RH experiments, it is possible that a small amount of water was retained in the particle phase (Ghorai et al., 2011; Lin et al., 2021) and available for catalyzing the decomposition of organic nitrates. Due to the diffusion limitations caused by high particle viscosity under ~~dry~~ low-RH conditions, some of the remaining organics after the decomposition of NF3 might stay in the samples and be grouped into any of the ~~non-nitrated organic~~CHO factors. As the ~~non-nitrated organic~~CHO factor F1 was in the volatility range between SVOCs and LVOCs, moderate evaporation could still take place in the timescale of 4.25 h even when the particle viscosity is high (Li et al., 2019). Therefore, the negligible change in the NCR of F1 (Figure 7b, red) cannot be explained without considering the additional formation of compounds (i.e., products from the decomposition of NF2 and/or NF3).

When large amounts of particulate water were present, the NCR values of NF1 – 3 distinctly changed with increasing evaporation. While NF1 displayed a significant increase in its NCR at the fresh stage under high-RH conditions, NF2 and NF3 showed notable decreases in their NCR. Since both NF2 and NF3 belonged to the LVOC and ELVOC ranges, very minor evaporation would be expected for them within the average timescale of 0.25 h at the fresh stage (Li et al., 2019). Thus, the pronounced reductions in their NCR were mostly driven by aqueous-phase processes. ~~Even though the NCR of NF2 and NF3 also showed a decreasing trend with increasing evaporation under dry conditions, we did not observe any production of compounds grouped into NF1 (Figure 5a) or an increase in its NCR (Figure 8b). One explanation for the difference in the NCR of NF1 could be that the functional groups involved in the decomposition process vary between the two evaporation stages (dry, RTC vs. high RH, fresh). As the produced organic nitrates are multifunctional, hydrolysis is not necessarily restricted to the nitrate groups under high RH conditions. Other functional groups like peroxides and esters can undergo hydrolysis as well. On the one hand, compounds in NF1 could be products from the decomposition of NF2 and NF3. On the other hand, they could be also formed via the nitration of alcohols with HNO_3 that could be produced from the decomposition of NF2 and NF3 (Wang et al., 2021).~~ When SOA particles continued to evaporate in the timescale of 4.25 h at high RH, compounds within the range of SVOCs could be possibly removed by evaporation due to their high C^* values. However, significant removal primarily due to evaporation would not be expected for those compounds in the range of LVOCs and ELVOCs (Li et al., 2019), unless other loss mechanisms (i.e., aqueous-phase process) exist. ~~As a majority of compounds in each organic nitrate factor were desorbed in this volatility range, their decreasing NCR values were highly likely caused by another loss process (i.e., aqueous-phase process) in addition to evaporation.~~

3.4.~~2~~ 3 Possible aqueous-phase processes affecting NCR of ~~non-nitrated organics~~ CHO compounds and ON

When compounds dissociate (here, mostly hydrolyze) into smaller molecules, the products of this process can either evaporate from or stay in the particle phase and possibly participate in further reactions with other molecules. Note that products that

evaporate do not contribute anymore to any of the factors. Linking two or more molecules via chemical bonds (accretion reactions) produces larger compounds of lower volatility which are less likely to evaporate. These products can undergo further reactions with increasing isothermal evaporation time especially in the presence of water. Note that if they have sufficiently low volatility, newly formed compounds from aqueous-phase processes will remain in the particle phase and contribute to other factors.

In the high-NO_x samples, only decreasing or constant NCR values were observed for factors F2 – F5 at the fresh stage under high-RH conditions. The formation pathways for products grouping into F3 and F5 are ~~minor~~minor since there was no increase in either of their NCR values. ~~-~~This additionally suggests that the reactions consuming F2 and F4 are mostly hydrolysis type processes ~~(i.e.,~~and create~~creating~~ products that do not remain in the particle phase~~)~~. ~~The formation pathways for products grouping into F3 and F5 are minor.~~ This formation of more volatile compounds may increase the observed isothermal evaporation of the particles. Under the same condition, NF2 and NF3 showed decreasing NCR values but NF1 exhibited an increase in its NCR. Even though the NCR of NF2 and NF3 also showed a decreasing trend with increasing evaporation at the RTC stage under low-RH conditions, we did not observe any production of compounds grouped into NF1 (Figure 5a) or an increase in its NCR (Figure 7b). One explanation for the difference in the NCR of NF1 could be that the functional groups involved in the decomposition process vary between the two evaporation stages (low RH, RTC vs. high RH, fresh). As the ON produced in the OFR are multifunctional, hydrolysis is not necessarily restricted to the nitrate groups under high-RH conditions. Other functional groups like peroxides and esters can undergo hydrolysis as well. Compounds in NF1 could be products from the decomposition of NF2 and NF3. It is also possible that compounds in NF1 could be formed via the nitration of alcohols in the presence of HNO_3 (Wang et al., 2021). While alcohols could be from CHO samples factors (e.g., F2, F4 and F5) that displayed decreasing NCR values, HNO_3 could be produced from the decomposition of NF2 and NF3 or already be present in the particles from uptake during the SOA formation in the OFR under high-NO_x conditions.

In the low-NO_x case, we observed factors with increasing NCR (F3 and F5) and with decreasing NCR (F2 and F4) when RH increased. It is likely that the particle-phase reactions involving compounds in F2 and/or F4 result in ~~low-~~low-volatility products contributed to F3 and F5. Hence, accretion type reactions must be the dominant pathway for this SOA type. Products from such accretion reactions could have sufficiently low volatility and slow down the particle evaporation, possibly resulting in the slightly larger VFR_{avg} in the low-NO_x case (Figure 7c). One possible type of accretion reaction could be the Baeyer – Villiger reaction of peroxides (e.g., peroxycarboxylic acid and hydroperoxide) (Lim and Turpin, 2015; Claflin et al., 2018) which are expected to be relatively more abundant for the low-NO_x samples of which $RO_2 + HO_2$ reactions were favored during SOA formation, compared to the high-NO_x samples (Ziemann and Atkinson, 2012; Peng and Jimenez, 2020). Note that $RO_2 + HO_2$ reactions can also lead to the production of carboxylic acids. Although we cannot rule out the occurrence of Fischer esterification requiring carboxylic acids, such reaction could not be observed even in extremely acidic particles for the relevant time scales of hours (Birdsall et al., 2013; Kristensen et al., 2014).

When particles continued to evaporate in the RTC under high-RH conditions, there were again differences in the evolution of F2 – F5 for low-NO_x and high-NO_x conditions. ~~While F2 and F4 displayed continuous decreases in NCR in the high-NO_x samples, these two factors experienced increases in their NCR in the low-NO_x ones.~~ While F2 and F4 experienced increases in their NCR in the low-NO_x samples, these two factors displayed continuous decreases in their NCR in the high-NO_x ones. For the three ON factors in the high-NO_x samples, they consistently showed decreasing NCR values, and also exhibited more significant decreases in their NCR values as compared with most of the CHO factors. As a majority of compounds in each ON factor were desorbed in the volatility range of LVOCs and ELVOCs, their decreasing NCR values were highly likely caused by aqueous-phase process instead of evaporation. Very likely, hydrolysis and accretion were the underlying reactions for the high-NO_x case, and those resulted products of sufficient low volatility possibly contributed to the constant and increasing NCR values of F3 and F5. ~~-~~For the high-NO_x samples, the important role of accretion at the RTC stage but not at the fresh stage

might indicate the timescale required for such reaction to be in the order of hours. Kinetic measurements have suggested that while the peroxy hemiacetal formation involving peroxides and carbonyls has a timescale from 1 min to 2h-, the formation of hemiacetal from reactions between alcohol and carbonyls is at least one order of magnitude slower (i.e., timescale of 10h) (Ziemann and Atkinson, 2012). Furthermore, the increasing NCR of F2 and F4 in the low-NO_x case was driven by the net production of compounds. This was likely attributed to the decomposition of compounds with short lifetime (e.g., acylperoxy hemiacetals and peroxy hemiacetals), originally (i.e., at the fresh stage) grouped into F3 and F5 (Claflin et al., 2018). Figure S13 in SI shows a graphical representation of the described processes occurring during the isothermal evaporation of α-pinene SOA particles under two high-RH evaporation stages (fresh vs RTC).

4 Conclusions

Many studies have focused on the impact of NO_x on the aerosol yield as well as gaseous and particulate products during SOA formation (Zhao et al., 2018; Pullinen et al., 2020). Our study is one of the few studies providing molecular-level information about particle-phase processes in SOA that were formed in the presence of NO_x. We examined the changes in volume and molecular composition of α-pinene SOA particles that were formed under low-NO_x and high-NO_x conditions during isothermal evaporation.

~~Although up~~ In the high-NO_x case, up to 20 wt % of the particle-phase material could be attributed to ~~organic nitrates~~ ON. In general, ON showed approximately 5 °C lower T_{50} and slightly higher volatility, compared with CHO compounds in the high-NO_x samples. Although the signal contribution of ON differed between the SOA particles that were formed under low- and high-NO_x conditions in the OFR, ~~in the high NO_x case~~, the overall particle volatility derived from isothermal evaporation and from FIGAERO-CIMS measurements was very similar for the two SOA types. Applying PMF to analyze the FIGAERO-CIMS thermal desorption data revealed distinct differences in the initial composition of both the particle and gas phase of the two SOA types for the ~~non-nitrated organic~~CHO compounds. These observations may be explained by that the effect of high NO_x concentrations during the oxidation of α-pinene goes beyond the formation of ~~organic nitrates~~ON. High NO_x concentrations could also suppress the formation of organic compounds (e.g., peroxide-containing compounds) from the RO_2 + HO_2 reaction pathways. Apart from competing with RO_2 + HO_2 reactions, recent work suggests that with increased NO_x emissions, the RO_2 + NO pathway can also surpass autoxidation reactions during the photooxidation of α-pinene and thus decrease the yield of highly oxygenated molecules (HOMs) (Pye et al., 2019). The majority of them partition into the particle phase due to their low volatilities (Mutzel et al., 2015). This change in HOM formation will both decrease the aerosol yield and change the composition of the formed SOA. HOMs often contain multiple peroxide functional groups (Bianchi et al., 2019). Thus, the reduction of HOM production will further lower the overall peroxide content of SOA particles together with the suppression of RO_2 + HO_2 reactions under high NO_x conditions.

At higher RH, both SOA types exhibited faster particle evaporation rates and lost a larger fraction of materials as compared to ~~dry~~ low-RH conditions. This agrees with previous studies showing that higher RH enhances particle evaporation (Yli-Juuti et al., 2017; Buchholz et al., 2019; Li et al., 2019). But in our study, we find that although the enhancement in isothermal evaporation was similar for both SOA types, the dominant aqueous-phase processes occurring in the particle phase were indeed different. I.e., the differences in the initial particle composition (e.g., the lower peroxide content for the high NO_x conditions) led to different chemical reactions occurring in the particle phase when particulate water was present. Many of the compounds involved in the aqueous-phase processes were of low or extremely low volatility, and hence did not evaporate in the RTC within the average experimental time scale of 4.25 h. This suggests that the observed process-level differences are potentially important for the fate of individual organic molecules in the particle phase, but their impact on overall particle volatility under ambient conditions might be negligible.

Interactions of BVOC emissions with high concentrations of NO_x are especially relevant in suburban areas. In such environments, the particle composition and aqueous-phase processes may be different from those found in low-NO_x environments, for instance in pristine forest areas where particulate samples should have higher peroxide contents (Surratt et al., 2006). In addition, particulate ON is highly prevalent in suburban areas, contributing on average 21% of non-refractory submicron particulate matter in mass (Kiendler-Scharr et al., 2016). ON can have sufficiently low volatility to remain in the particle phase. On the other hand, ON is effectivity water-labile and very likely undergoes hydrolysis at the atmospheric-relevant RH (> 40%). Therefore, ON which has low volatility can still be removed from the particle phase, when being hydrolyzed into smaller products that have higher volatility. As our findings are limited to the aqueous-phase process in α-pinene SOA particles, future studies on other BVOC systems and even emissions from urban vegetation are needed to estimate the overall importance of these processes and how they may affect other physicochemical properties of SOA particles.

Data availability. The data set is available upon request from Annele Virtanen (annele.virtanen@uef.fi).

Supplement. The supplement related to this article is available online.

Author contribution. ZL, AB, and AV designed the study. ZL, AB, LB, AY, and LH carried out laboratory experiments. ZL, AB, LH, IP, SS, and AV performed data analysis and interpretation. ZL wrote the paper with contributions from all coauthors.

Competing interests. The authors declare that they have no conflict of interest.

Acknowledgements. This research has been supported by the Academy of Finland (grant nos. 299544, 310682, 307331, and 317373), the Itä-Suomen Yliopisto (Doctoral Programme in Environmental Physics, Health and Biology), and FP7 Ideas: European Research Council (QAPPA, grant no. 335478).

References

Barreira, L. M. F., Ylisirnio, A., Pullinen, I., Buchholz, A., Li, Z. J., Lipp, H., Junninen, H., Horrak, U., Noe, S. M., Krasnova, A., Krasnov, D., Kask, K., Talts, E., Niinemets, U., Ruiz-Jimenez, J., and Schobesberger, S.: The importance of sesquiterpene oxidation products for secondary organic aerosol formation in a springtime hemiboreal forest, Atmos. Chem. Phys., 21, 11781-11800, 10.5194/acp-21-11781-2021, 2021.

Bianchi, F., Kurten, T., Riva, M., Mohr, C., Rissanen, M. P., Roldin, P., Berndt, T., Crounse, J. D., Wennberg, P. O., Mentel, T. F., Wildt, J., Junninen, H., Jokinen, T., Kulmala, M., Worsnop, D. R., Thornton, J. A., Donahue, N., Kjaergaard, H. G., and Ehn, M.: Highly oxygenated organic molecules (HOM) from gas-phase autoxidation involving peroxy radicals: A key contributor to atmospheric aerosol, Chem. Rev., 119, 3472-3509, 10.1021/acs.chemrev.8b00395, 2019.

Birdsall, A. W., Zentner, C. A., and Elrod, M. J.: Study of the kinetics and equilibria of the oligomerization reactions of 2-methylglyceric acid, Atmos. Chem. Phys., 13, 3097-3109, 10.5194/acp-13-3097-2013, 2013.

Buchholz, A., Ylisirniö, A., Huang, W., Mohr, C., Canagaratna, M., Worsnop, D. R., Schobesberger, S., and Virtanen, A.: Deconvolution of FIGAERO–CIMS thermal desorption profiles using positive matrix factorisation to identify chemical and physical processes during particle evaporation, Atmos. Chem. Phys., 20, 7693-7716, 2020.

Buchholz, A., Lambe, A. T., Ylisirniö, A., Li, Z., Tikkanen, O.-P., Faiola, C., Kari, E., Hao, L., Luoma, O., Huang, W., Mohr, C., Worsnop, D. R., Nizkorodov, S. A., Yli-Juuti, T., Schobesberger, S., and Virtanen, A.: Insights into the O : C-dependent mechanisms controlling the evaporation of α-pinene secondary organic aerosol particles, Atmos. Chem. Phys., 19, 4061-4073, 10.5194/acp-19-4061-2019, 2019.

Canagaratna, M. R., Jimenez, J. L., Kroll, J. H., Chen, Q., Kessler, S. H., Massoli, P., Hildebrandt Ruiz, L., Fortner, E., Williams, L. R., Wilson, K. R., Surratt, J. D., Donahue, N. M., Jayne, J. T., and Worsnop, D. R.: Elemental ratio measurements of organic compounds using aerosol mass spectrometry: Characterization, improved calibration, and implications, Atmos. Chem. Phys., 15, 253-272, 10.5194/acp-15-253-2015, 2015.

Claflin, M. S., Krechmer, J. E., Hu, W., Jimenez, J. L., and Ziemann, P. J.: Functional group composition of secondary organic aerosol formed from ozonolysis of α-pinene under high VOC and autoxidation conditions, ACS Earth and Space Chemistry, 2, 1196-1210, 2018.

D'Ambro, E. L., Lee, B. H., Liu, J., Shilling, J. E., Gaston, C. J., Lopez-Hilfiker, F. D., Schobesberger, S., Zaveri, R. A., Mohr, C., and Lutz, A.: Molecular composition and volatility of isoprene photochemical oxidation secondary organic aerosol under low-and high-no x conditions, Atmos. Chem. Phys., 17, 159-174, 2017.

D'Ambro, E. L., Schobesberger, S., Zaveri, R. A., Shilling, J. E., Lee, B. H., Lopez-Hilfiker, F. D., Mohr, C., and Thornton, J. A.: Isothermal evaporation of α-Pinene ozonolysis SOA: Volatility, phase state, and oligomeric composition, ACS Earth and Space Chemistry, 2, 1058-1067, 10.1021/acsearthspacechem.8b00084, 2018.

Donahue, N. M., Kroll, J. H., Pandis, S. N., and Robinson, A. L.: A two-dimensional volatility basis set – Part 2: Diagnostics of organic-aerosol evolution, Atmos. Chem. Phys., 12, 615-634, 10.5194/acp-12-615-2012, 2012.

Donahue, N. M., Robinson, A. L., Stanier, C. O., and Pandis, S. N.: Coupled partitioning, dilution, and chemical aging of semivolatile organics, Environ. Sci. Technol., 40, 2635-2643, 10.1021/es052297c, 2006.

Duncan, B. N., Lamsal, L. N., Thompson, A. M., Yoshida, Y., Lu, Z., Streets, D. G., Hurwitz, M. M., and Pickering, K. E.: A space-based, high-resolution view of notable changes in urban NO_x pollution around the world (2005–2014), Journal of Geophysical Research: Atmospheres, 121, 976-996, 2016.

Ehn, M., Thornton, J. A., Kleist, E., Sipila, M., Junninen, H., Pullinen, I., Springer, M., Rubach, F., Tillmann, R., Lee, B., Lopez-Hilfiker, F., Andres, S., Acir, I. H., Rissanen, M., Jokinen, T., Schobesberger, S., Kangasluoma, J., Kontkanen, J., Nieminen, T., Kurten, T., Nielsen, L. B., Jorgensen, S., Kjaergaard, H. G., Canagaratna, M., Maso, M. D., Berndt, T., Petaja, T., Wahner, A., Kerminen, V. M., Kulmala, M., Worsnop, D. R., Wildt, J., and Mentel, T. F.: A large source of low-volatility secondary organic aerosol, Nature, 506, 476-479, 10.1038/nature13032, 2014.

Francisco, M. A. and Krylowski, J.: Chemistry of organic nitrates: Thermal chemistry of linear and branched organic nitrates, Industrial & Engineering Chemistry Research, 44, 5439-5446, 10.1021/ie049380d, 2005.

Ghorai, S., Laskin, A., and Tivanski, A. V.: Spectroscopic evidence of keto-enol tautomerism in deliquesced malonic acid particles, J. Phys. Chem. A, 115, 4373-4380, 10.1021/jp112360x, 2011.

Guenther, A., Hewitt, C. N., Erickson, D., Fall, R., Geron, C., Graedel, T., Harley, P., Klinger, L., Lerdau, M., Mckay, W. A., Pierce, T., Scholes, B., Steinbrecher, R., Tallamraju, R., Taylor, J., and Zimmerman, P.: A global-model of natural volatile organic-compound emissions, J Geophys Res-Atmos, 100, 8873-8892, Doi 10.1029/94jd02950, 1995.

Guenther, A. B., Jiang, X., Heald, C. L., Sakulyanontvittaya, T., Duhl, T., Emmons, L. K., and Wang, X.: The model of emissions of gases and aerosols from nature version 2.1 (MEGAN2.1): An extended and updated framework for modeling biogenic emissions, Geoscientific Model Development, 5, 1471-1492, 10.5194/gmd-5-1471-2012, 2012.

Hodzic, A., Kasibhatla, P. S., Jo, D. S., Cappa, C. D., Jimenez, J. L., Madronich, S., and Park, R. J.: Rethinking the global secondary organic aerosol (SOA) budget: Stronger production, faster removal, shorter lifetime, Atmos. Chem. Phys., 16, 7917-7941, 10.5194/acp-16-7917-2016, 2016.

Huang, W., Saathoff, H., Shen, X., Ramisetty, R., Leisner, T., and Mohr, C.: Chemical characterization of highly functionalized organonitrates contributing to night-time organic aerosol mass loadings and particle growth, Environ. Sci. Technol., 53, 1165-1174, 10.1021/acs.est.8b05826, 2019.

Hyttinen, N., Pullinen, I., Nissinen, A., Schobesberger, S., Virtanen, A., and Yli-Juuti, T.: Comparison of saturation vapor pressures of α-pinene+o_3 oxidation products derived from COSMO-RS computations and thermal desorption experiments, Atmos. Chem. Phys., 22, 1195-1208, 2022.

Jokinen, T., Berndt, T., Makkonen, R., Kerminen, V. M., Junninen, H., Paasonen, P., Stratmann, F., Herrmann, H., Guenther, A. B., Worsnop, D. R., Kulmala, M., Ehn, M., and Sipila, M.: Production of extremely low volatile organic compounds from biogenic emissions: Measured yields and atmospheric implications, Proc. Natl. Acad. Sci. U. S. A., 112, 7123-7128, 10.1073/pnas.1423977112, 2015.

Kang, E., Root, M. J., Toohey, D. W., and Brune, W. H.: Introducing the concept of potential aerosol mass (PAM), Atmos. Chem. Phys., 7, 5727-5744, DOI 10.5194/acp-7-5727-2007, 2007.

Kari, E., Miettinen, P., Yli-Pirila, P., Virtanen, A., and Faiola, C. L.: PTR-ToF-MS product ion distributions and humidity-dependence of biogenic volatile organic compounds, Int. J. Mass spectrom., 430, 87-97, 10.1016/j.ijms.2018.05.003, 2018.

Kiendler-Scharr, A., Mensah, A. A., Friese, E., Topping, D., Nemitz, E., Prevot, A. S. H., Aijala, M., Allan, J., Canonaco, F., Canagaratna, M., Carbone, S., Crippa, M., Dall Osto, M., Day, D. A., De Carlo, P., Di Marco, C. F., Elbern, H., Eriksson, A., Freney, E., Hao, L., Herrmann, H., Hildebrandt, L., Hillamo, R., Jimenez, J. L., Laaksonen, A., McFiggans, G., Mohr, C., O'Dowd, C., Otjes, R., Ovadnevaite, J., Pandis, S. N., Poulain, L., Schlag, P., Sellegri, K., Swietlicki, E., Tiitta, P., Vermeulen, A., Wahner, A., Worsnop, D., and Wu, H. C.: Ubiquity of organic nitrates from nighttime chemistry in the European submicron aerosol, Geophys. Res. Lett., 43, 7735-7744, 10.1002/2016gl069239, 2016.

Kristensen, K., Cui, T., Zhang, H., Gold, A., Glasius, M., and Surratt, J.: Dimers in α-pinene secondary organic aerosol: Effect of hydroxyl radical, ozone, relative humidity and aerosol acidity, Atmos. Chem. Phys., 14, 4201-4218, 2014.

Kroll, J. H. and Seinfeld, J. H.: Chemistry of secondary organic aerosol: Formation and evolution of low-volatility organics in the atmosphere, Atmos. Environ., 42, 3593-3624, 10.1016/j.atmosenv.2008.01.003, 2008.

Kuwata, M., Zorn, S. R., and Martin, S. T.: Using elemental ratios to predict the density of organic material composed of carbon, hydrogen, and oxygen, Environ. Sci. Technol., 46, 787-794, 10.1021/es202525q, 2012.

Lambe, A., Massoli, P., Zhang, X., Canagaratna, M., Nowak, J., Daube, C., Yan, C., Nie, W., Onasch, T., and Jayne, J.: Controlled nitric oxide production via $O(^1D)$+ N_2O reactions for use in oxidation flow reactor studies, Atmos. Meas. Tech., 10, 2283-2298, 2017.

Lambe, A. T., Onasch, T. B., Massoli, P., Croasdale, D. R., Wright, J. P., Ahern, A. T., Williams, L. R., Worsnop, D. R., Brune, W. H., and Davidovits, P.: Laboratory studies of the chemical composition and cloud condensation nuclei (CCN) activity of secondary organic aerosol (SOA) and oxidized primary organic aerosol (OPOA), Atmos. Chem. Phys., 11, 8913-8928, 10.5194/acp-11-8913-2011, 2011.

Lee, B. H., D'Ambro, E. L., Lopez-Hilfiker, F. D., Schobesberger, S., Mohr, C., Zawadowicz, M. A., Liu, J., Shilling, J. E., Hu, W., Palm, B. B., Jimenez, J. L., Hao, L., Virtanen, A., Zhang, H., Goldstein, A. H., Pye, H. O. T., and Thornton, J. A.: Resolving ambient organic aerosol formation and aging pathways with simultaneous molecular composition and volatility observations, ACS Earth Space Chem, 4, 391-402, 10.1021/acsearthspacechem.9b00302, 2020.

Lehtinen, K. E. J. and Kulmala, M.: A model for particle formation and growth in the atmosphere with molecular resolution in size, Atmos. Chem. Phys., 3, 251-257, DOI 10.5194/acp-3-251-2003, 2003.

Li, W. L. and Chen, D. R.: Performance of Nano-DMA operated with different gases for sheath and aerosol carrier flows, Aerosol Science and Technology, 39, 931-940, 10.1080/02786820500346520, 2005.

Li, Y. and Shiraiwa, M.: Timescales of secondary organic aerosols to reach equilibrium at various temperatures and relative humidities, Atmos. Chem. Phys., 19, 5959-5971, 10.5194/acp-19-5959-2019, 2019.

Li, Z., Tikkanen, O.-P., Buchholz, A., Hao, L., Kari, E., Yli-Juuti, T., and Virtanen, A.: Effect of decreased temperature on the evaporation of α-Pinene secondary organic aerosol particles, ACS Earth and Space Chemistry, 3, 2775-2785, 10.1021/acsearthspacechem.9b00240, 2019.

Li, Z., Buchholz, A., Ylisirniö, A., Barreira, L., Hao, L., Schobesberger, S., Yli-Juuti, T., and Virtanen, A.: Evolution of volatility and composition in sesquiterpene-mixed and α-pinene secondary organic aerosol particles during isothermal evaporation, Atmos. Chem. Phys., 21, 18283-18302, 10.5194/acp-21-18283-2021, 2021.

Lihavainen, H., Asmi, E., Aaltonen, V., Makkonen, U., and Kerminen, V. M.: Direct radiative feedback due to biogenic secondary organic aerosol estimated from boreal forest site observations, Environmental Research Letters, 10, 104005, 10.1088/1748-9326/10/10/104005, 2015.

Lim, Y. B. and Turpin, B. J.: Laboratory evidence of organic peroxide and peroxyhemiacetal formation in the aqueous phase and implications for aqueous OH, Atmos. Chem. Phys., 15, 12867-12877, 10.5194/acp-15-12867-2015, 2015.

Lin, J. J., Raj, R. K., Wang, S., Kokkonen, E., Mikkela, M. H., Urpelainen, S., and Prisle, N. L.: Pre-deliquescent water uptake in deposited nanoparticles observed with in situ ambient pressure X-ray photoelectron spectroscopy, Atmos. Chem. Phys., 21, 4709-4727, 10.5194/acp-21-4709-2021, 2021.

Lopez-Hilfiker, F., Mohr, C., Ehn, M., Rubach, F., Kleist, E., Wildt, J., Mentel, T. F., Carrasquillo, A., Daumit, K., and Hunter, J.: Phase partitioning and volatility of secondary organic aerosol components formed from α-pinene ozonolysis and OH oxidation: The importance of accretion products and other low volatility compounds, Atmos. Chem. Phys., 15, 7765-7776, 2015.

Lopez-Hilfiker, F. D., Mohr, C., Ehn, M., Rubach, F., Kleist, E., Wildt, J., Mentel, T. F., Lutz, A., Hallquist, M., Worsnop, D., and Thornton, J. A.: A novel method for online analysis of gas and particle composition: Description and evaluation of a filter inlet for gases and aerosols (FIGAERO), Atmos. Meas. Tech., 7, 983-1001, 10.5194/amt-7-983-2014, 2014.

Mitchell, L. E., Lin, J. C., Bowling, D. R., Pataki, D. E., Strong, C., Schauer, A. J., Bares, R., Bush, S. E., Stephens, B. B., Mendoza, D., Mallia, D., Holland, L., Gurney, K. R., and Ehleringer, J. R.: Long-term urban carbon dioxide observations reveal spatial and temporal dynamics related to urban characteristics and growth, Proc. Natl. Acad. Sci. U. S. A., 115, 2912-2917, 10.1073/pnas.1702393115, 2018.

Mohr, C., Thornton, J. A., Heitto, A., Lopez-Hilfiker, F. D., Lutz, A., Riipinen, I., Hong, J., Donahue, N. M., Hallquist, M., Petaja, T., Kulmala, M., and Yli-Juuti, T.: Molecular identification of organic vapors driving atmospheric nanoparticle growth, Nat Commun, 10, 4442, 10.1038/s41467-019-12473-2, 2019.

Mutzel, A., Poulain, L., Berndt, T., Iinuma, Y., Rodigast, M., Boge, O., Richters, S., Spindler, G., Sipila, M., Jokinen, T., Kulmala, M., and Herrmann, H.: Highly oxidized multifunctional organic compounds observed in tropospheric particles: A field and laboratory study, Environ. Sci. Technol., 49, 7754-7761, 10.1021/acs.est.5b00885, 2015.

Myhre, G., Shindell, D., Bréon, F., Collins, W., Fuglestvedt, J., Huang, J., Koch, D., Lamarque, J., Lee, D., and Mendoza, B.: Anthropogenic and natural radiative forcing. In: Climate change 2013: The physical science basis. Contribution of working group i to the fifth assessment report of the Intergovernmental Panel on Climate Change, Cambridge University Press, Cambridge, United Kingdom and New York, NY, USA, 659–740, 2013.

Paatero, P. and Tapper, U.: Positive matrix factorization: A non-negative factor model with optimal utilization of error estimates of data values, Environmetrics, 5, 111-126, 1994.

Peng, Z. and Jimenez, J. L.: Kinsim: A research-grade, user-friendly, visual kinetics simulator for chemical-kinetics and environmental-chemistry teaching, 2019.

Peng, Z. and Jimenez, J. L.: Radical chemistry in oxidation flow reactors for atmospheric chemistry research, Chem. Soc. Rev., 49, 2570-2616, 10.1039/c9cs00766k, 2020.

Peng, Z., Lee-Taylor, J., Orlando, J. J., Tyndall, G. S., and Jimenez, J. L.: Organic peroxy radical chemistry in oxidation flow reactors and environmental chambers and their atmospheric relevance, Atmos. Chem. Phys., 19, 813-834, 2019.

Priestley, M., Bannan, T. J., Le Breton, M., Worrall, S. D., Kang, S., Pullinen, I., Schmitt, S., Tillmann, R., Kleist, E., Zhao, D., Wildt, J., Garmash, O., Mehra, A., Bacak, A., Shallcross, D. E., Kiendler-Scharr, A., Hallquist, A. M., Ehn, M., Coe, H., Percival, C. J., Hallquist, M., Mentel, T. F., and McFiggans, G.: Chemical characterisation of benzene oxidation products under high- and low-NO_x conditions using chemical ionisation mass spectrometry, Atmos. Chem. Phys., 21, 3473-3490, 10.5194/acp-21-3473-2021, 2021.

Pullinen, I., Schmitt, S., Kang, S., Sarrafzadeh, M., Schlag, P., Andres, S., Kleist, E., Mentel, T. F., Rohrer, F., and Springer, M.: Impact of NO_x on secondary organic aerosol (SOA) formation from α-pinene and β-pinene photooxidation: The role of highly oxygenated organic nitrates, Atmos. Chem. Phys., 20, 10125-10147, 2020.

Pye, H. O. T., D'Ambro, E. L., Lee, B. H., Schobesberger, S., Takeuchi, M., Zhao, Y., Lopez-Hilfiker, F., Liu, J., Shilling, J. E., Xing, J., Mathur, R., Middlebrook, A. M., Liao, J., Welti, A., Graus, M., Warneke, C., de Gouw, J. A., Holloway, J. S., Ryerson, T. B., Pollack, I. B., and Thornton, J. A.: Anthropogenic enhancements to production of highly oxygenated molecules from autoxidation, Proc. Natl. Acad. Sci. U. S. A., 116, 6641-6646, 10.1073/pnas.1810774116, 2019.

Ranney, A. P. and Ziemann, P. J.: Kinetics of acid-catalyzed dehydration of cyclic hemiacetals in organic aerosol particles in equilibrium with nitric acid vapor, J. Phys. Chem. A, 120, 2561-2568, 10.1021/acs.jpca.6b01402, 2016.

Saukko, E., Lambe, A. T., Massoli, P., Koop, T., Wright, J. P., Croasdale, D. R., Pedernera, D. A., Onasch, T. B., Laaksonen, A., Davidovits, P., Worsnop, D. R., and Virtanen, A.: Humidity-dependent phase state of SOA particles from biogenic and anthropogenic precursors, Atmos. Chem. Phys., 12, 7517-7529, 10.5194/acp-12-7517-2012, 2012.

Sporre, M. K., Swietlicki, E., Glantz, P., and Kulmala, M.: A long-term satellite study of aerosol effects on convective clouds in nordic background air, Atmos. Chem. Phys., 14, 2203-2217, 10.5194/acp-14-2203-2014, 2014.

Sporre, M. K., Blichner, S. M., Karset, I. H., Makkonen, R., and Berntsen, T. K.: BVOC–aerosol–climate feedbacks investigated using noresm, Atmos. Chem. Phys., 19, 4763-4782, 2019.

Surratt, J. D., Murphy, S. M., Kroll, J. H., Ng, N. L., Hildebrandt, L., Sorooshian, A., Szmigielski, R., Vermeylen, R., Maenhaut, W., Claeys, M., Flagan, R. C., and Seinfeld, J. H.: Chemical composition of secondary organic aerosol formed from the photooxidation of isoprene, J. Phys. Chem. A, 110, 9665-9690, 10.1021/jp061734m, 2006.

Tikkanen, O.-P., Buchholz, A., Ylisirniö, A., Schobesberger, S., Virtanen, A., and Yli-Juuti, T.: Comparing secondary organic aerosol (SOA) volatility distributions derived from isothermal SOA particle evaporation data and FIGAERO–CIMS measurements, Atmos. Chem. Phys., 20, 10441-10458, 2020.

Tunved, P., Hansson, H. C., Kerminen, V. M., Strom, J., Maso, M. D., Lihavainen, H., Viisanen, Y., Aalto, P. P., Komppula, M., and Kulmala, M.: High natural aerosol loading over boreal forests, Science, 312, 261-263, 10.1126/science.1123052, 2006.

Ulbrich, I. M., Canagaratna, M. R., Zhang, Q., Worsnop, D. R., and Jimenez, J. L.: Interpretation of organic components from positive matrix factorization of aerosol mass spectrometric data, Atmos. Chem. Phys., 9, 2891-2918, 10.5194/acp-9-2891-2009, 2009.

Vaden, T. D., Imre, D., Beranek, J., Shrivastava, M., and Zelenyuk, A.: Evaporation kinetics and phase of laboratory and ambient secondary organic aerosol, Proc. Natl. Acad. Sci. U. S. A., 108, 2190-2195, 10.1073/pnas.1013391108, 2011.

Virtanen, A., Joutsensaari, J., Koop, T., Kannosto, J., Yli-Pirila, P., Leskinen, J., Makela, J. M., Holopainen, J. K., Poschl, U., Kulmala, M., Worsnop, D. R., and Laaksonen, A.: An amorphous solid state of biogenic secondary organic aerosol particles, Nature, 467, 824-827, 10.1038/nature09455, 2010.

Wang, Y., Piletic, I. R., Takeuchi, M., Xu, T., France, S., and Ng, N. L.: Synthesis and hydrolysis of atmospherically relevant monoterpene-derived organic nitrates, Environ. Sci. Technol., 55, 14595-14606, 10.1021/acs.est.1c05310, 2021.

Xu, L., Guo, H., Boyd, C. M., Klein, M., Bougiatioti, A., Cerully, K. M., Hite, J. R., Isaacman-VanWertz, G., Kreisberg, N. M., Knote, C., Olson, K., Koss, A., Goldstein, A. H., Hering, S. V., de Gouw, J., Baumann, K., Lee, S. H., Nenes, A., Weber, R. J., and Ng, N. L.: Effects of anthropogenic emissions on aerosol formation from isoprene and monoterpenes in the southeastern united states, Proc. Natl. Acad. Sci. U. S. A., 112, 37-42, 10.1073/pnas.1417609112, 2015.

Yli-Juuti, T., Pajunoja, A., Tikkanen, O. P., Buchholz, A., Faiola, C., Vaisanen, O., Hao, L., Kari, E., Perakyla, O., Garmash, O., Shiraiwa, M., Ehn, M., Lehtinen, K., and Virtanen, A.: Factors controlling the evaporation of secondary organic aerosol from alpha-pinene ozonolysis, Geophys. Res. Lett., 44, 2562-2570, 10.1002/2016GL072364, 2017.

Yli-Juuti, T., Mielonen, T., Heikkinen, L., Arola, A., Ehn, M., Isokaanta, S., Keskinen, H. M., Kulmala, M., Laakso, A., Lipponen, A., Luoma, K., Mikkonen, S., Nieminen, T., Paasonen, P., Petaja, T., Romakkaniemi, S., Tonttila, J., Kokkola, H., and Virtanen, A.: Significance of the organic aerosol driven climate feedback in the boreal area, Nat Commun, 12, 5637, 10.1038/s41467-021-25850-7, 2021.

Ylisirniö, A., Barreira, L. M. F., Pullinen, I., Buchholz, A., Jayne, J., Krechmer, J. E., Worsnop, D. R., Virtanen, A., and Schobesberger, S.: On the calibration of FIGAERO-ToF-CIMS: Importance and impact of calibrant delivery for the particle-phase calibration, Atmos. Meas. Tech., 14, 355-367, 10.5194/amt-14-355-2021, 2021.

Ylisirniö, A., Buchholz, A., Mohr, C., Li, Z. J., Barreira, L., Lambe, A., Faiola, C., Kari, E., Yli-Juuti, T., Nizkorodov, S. A., Worsnop, D. R., Virtanen, A., and Schobesberger, S.: Composition and volatility of secondary organic aerosol (SOA) formed from oxidation of real tree emissions compared to simplified volatile organic compound (VOC) systems, Atmos. Chem. Phys., 20, 5629-5644, 10.5194/acp-20-5629-2020, 2020.

Zare, A., Fahey, K. M., Sarwar, G., Cohen, R. C., and Pye, H. O. T.: Vapor-pressure pathways initiate but hydrolysis products dominate the aerosol estimated from organic nitrates, ACS Earth Space Chem, 3, 1426-1437, 10.1021/acsearthspacechem.9b00067, 2019.

Zare, A., Romer, P. S., Nguyen, T., Keutsch, F. N., Skog, K., and Cohen, R. C.: A comprehensive organic nitrate chemistry: Insights into the lifetime of atmospheric organic nitrates, Atmos. Chem. Phys., 18, 15419-15436, 10.5194/acp-18-15419-2018, 2018.

Zaveri, R. A., Shilling, J. E., Zelenyuk, A., Zawadowicz, M. A., Suski, K., China, S., Bell, D. M., Veghte, D., and Laskin, A.: Particle-phase diffusion modulates partitioning of semivolatile organic compounds to aged secondary organic aerosol, Environ. Sci. Technol., 54, 2595-2605, 10.1021/acs.est.9b05514, 2020.

Zhang, H., Yee, L. D., Lee, B. H., Curtis, M. P., Worton, D. R., Isaacman-VanWertz, G., Offenberg, J. H., Lewandowski, M., Kleindienst, T. E., Beaver, M. R., Holder, A. L., Lonneman, W. A., Docherty, K. S., Jaoui, M., Pye, H. O. T., Hu, W., Day, D. A., Campuzano-Jost, P., Jimenez, J. L., Guo, H., Weber, R. J., de Gouw, J., Koss, A. R., Edgerton, E. S., Brune, W., Mohr, C., Lopez-Hilfiker, F. D., Lutz, A., Kreisberg, N. M., Spielman, S. R., Hering, S. V., Wilson, K. R., Thornton, J. A., and Goldstein, A. H.: Monoterpenes are the largest source of summertime organic aerosol in the southeastern united states, Proc. Natl. Acad. Sci. U. S. A., 115, 2038-2043, 10.1073/pnas.1717513115, 2018.

Zhao, D., Schmitt, S. H., Wang, M., Acir, I.-H., Tillmann, R., Tan, Z., Novelli, A., Fuchs, H., Pullinen, I., and Wegener, R.: Effects of NO_x and SO_2 on the secondary organic aerosol formation from photooxidation of α-pinene and limonene, Atmos. Chem. Phys., 18, 1611-1628, 2018.

Ziemann, P. J. and Atkinson, R.: Kinetics, products, and mechanisms of secondary organic aerosol formation, Chem. Soc. Rev., 41, 6582-6605, 10.1039/c2cs35122f, 2012.

Table 1~~1~~. Mass contribution of ~~non-nitrated organics~~CHO compounds and ~~organic nitrates~~ON to α-pinene SOA particle samples under high-NO_x conditions.

Particle Sample	Instrument	Method	~~Non-nitrated organics~~CHO compounds (wt %)	~~Organic nitrates~~ON (wt %)
~~Dry~~ Low RH, Fresh	FIGAERO-CIMS		82	18
	AMS [a]	NO_2^+/NO^+ [b]	92	7
		ON_{max} [c]	89	11
~~Dry~~ Low RH, RTC	FIGAERO-CIMS		86	14
	AMS		N/A	N/A
Intermediate RH, Fresh	FIGAERO-CIMS		N/A	N/A
	AMS	NO_2^+/NO^+	90	9
		ON_{max}	88	12
High RH, Fresh	FIGAERO-CIMS		82	18
	AMS	NO_2^+/NO^+	79	19
		ON_{max}	77	23
High RH, RTC	FIGAERO-CIMS		93	7
	AMS		N/A	N/A

[a] For AMS methods, the average molecular weight of ~~organic nitrates~~ ON estimated from the FIGAERO – CIMS data was used.

[b] NO_2^+/NO^+: Estimating ~~organic nitrate~~ ON contribution using the difference in fragmentation between organic and inorganic nitrate species (Kiendler-Scharr et al., 2016).

[c] ON_{max}: Assuming that all nitrate moieties detected in the AMS were from organic nitrates.

Table 2~~2~~. Summary of ~~non-nitrated organic~~CHO factors in α-pinene SOA particle ~~samples~~ formed under low-NO_x and high-NO_x conditions in the OFR.

ID	Composition	OS_c [a]	MW / g mol^{-1}	T_{50} and interquartile range of ~~T_{desorp}~~ T_{desorp} [b]	
				Low-NO_x	High-NO_x
F1	$C_{6.9}H_{9.8}O_{4.9}$	0.21	171.05	76.07 [65.70, 92.53]	69.03 [60.93, 78.08]
F2	$C_{7.7}H_{10.1}O_{5.6}$	0.25	192.15	103.15 [88.42, 122.45]	95.42 [82.71, 110.30]
F3	$C_{8.7}H_{12.8}O_{5.4}$	-0.13	203.67	103.68 [89.24, 130.50]	99.78 [82.03, 128.14]
F4	$C_{10.9}H_{14.5}O_{7.1}$	0.07	258.98	136.70 [119.99, 156.37]	138.37 [119.96, 159.14]
F5	$C_8H_{10.8}O_{5.4}$	0.18	193.26	146.57 [123.89, 168.13]	157.43 [140.78, 173.65]
NF1	$C_{8.5}H_{13.1}NO_{6.9}$	-0.49	239.57	N/A	109.11 [92.45, 136.84]
NF2	$C_{8.7}H_{12.8}NO_{7.4}$	-0.31	249.67	N/A	86.14 [72.49, 99.29]
NF3	$C_{9.4}H_{14.2}N_{1.1}O_{7.9}$	-0.35	268.87	N/A	141.68 [126.09, 161.11]

[a] Values of OS_c for NF1-3 were calculated under the assumption that all nitrogen existed in the form of alkyl nitrates (Priestley et al., 2021).

[b] Values of T_{50} and interquartile range of T_{desorp} were determined with the ~~dry~~low-RH, fresh samples.

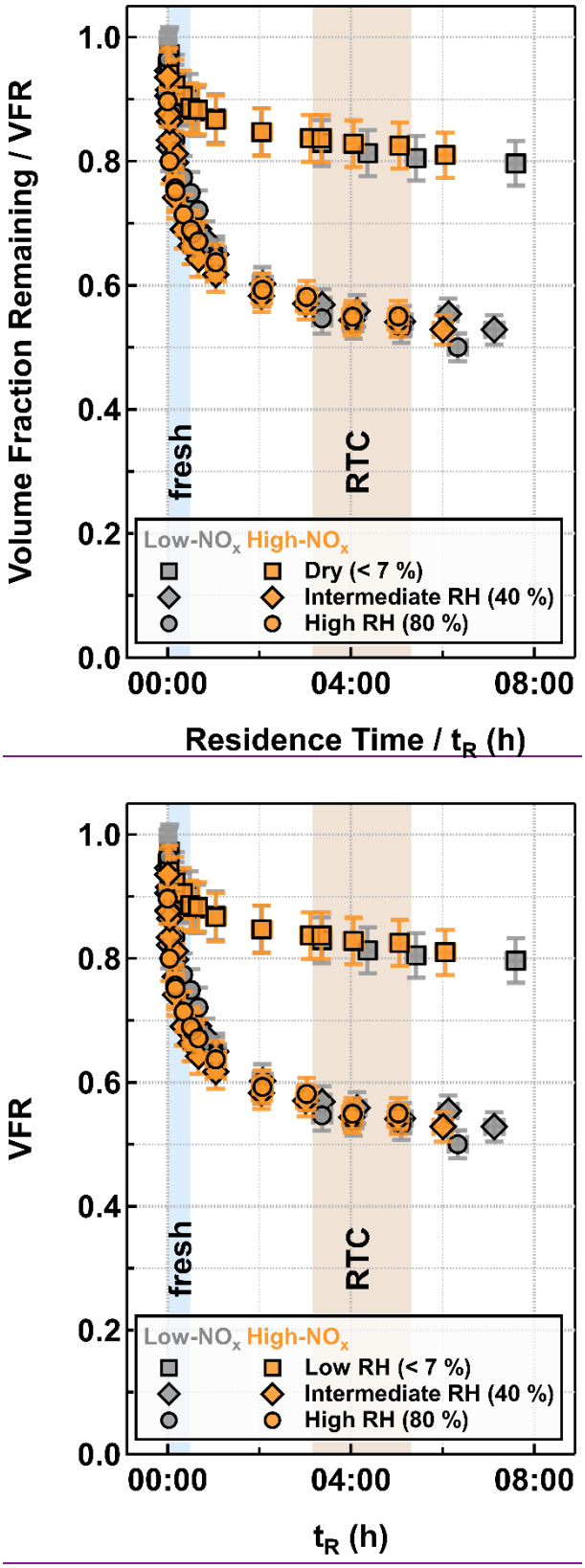

Figure 11. ~~Evapograms~~ Volume Fraction Remaining (VFR) derived from particle size measurements ~~for~~ as function of residence time (t_R) in the RTC ~~low-NO_x (grey) and high-NO_x (orange) cases~~ for α-pinene SOA particles which were formed under low-NO_x (grey) and high-NO_x (orange) conditions in the OFR and evaporated under ~~dry~~ low-RH (< 7 %, squares), ~~intermediate~~ intermediate-RH (40 % RH, diamonds) and ~~high~~ high-RH (80 % RH, circles) conditions. The blue and brown areas indicate the collection periods of FIGAERO-CIMS corresponding to fresh and RTC samples.

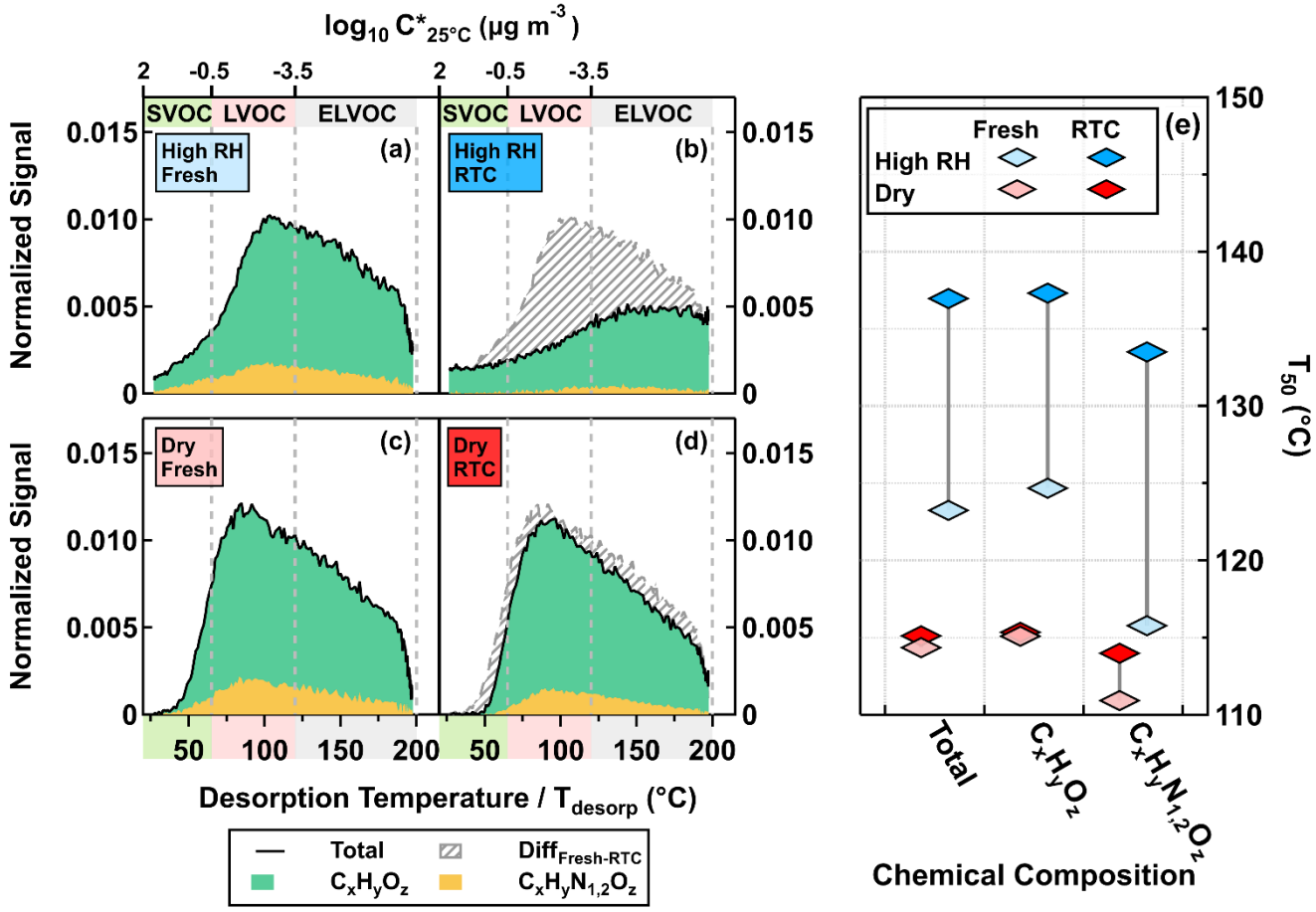
log10 C*25°C (μg m-3)
2 -0.5 -3.5
SVOC LVOC ELVOC
High RH Fresh
(a)
High RH RTC
(b)
Dry Fresh
(c)
Dry RTC
(d)
Normalized Signal
0.015
0.010
0.005
0
50 100 150 200
Desorption Temperature / Tdesorp (°C)
Total
CxHyOz
Diff Fresh-RTC
CxHyN1,2Oz
Fresh
RTC
High RH
Dry
(e)
T50 (°C)
150
140
130
120
110
Total
CxHyOz
CxHyN1,2Oz
Chemical Composition

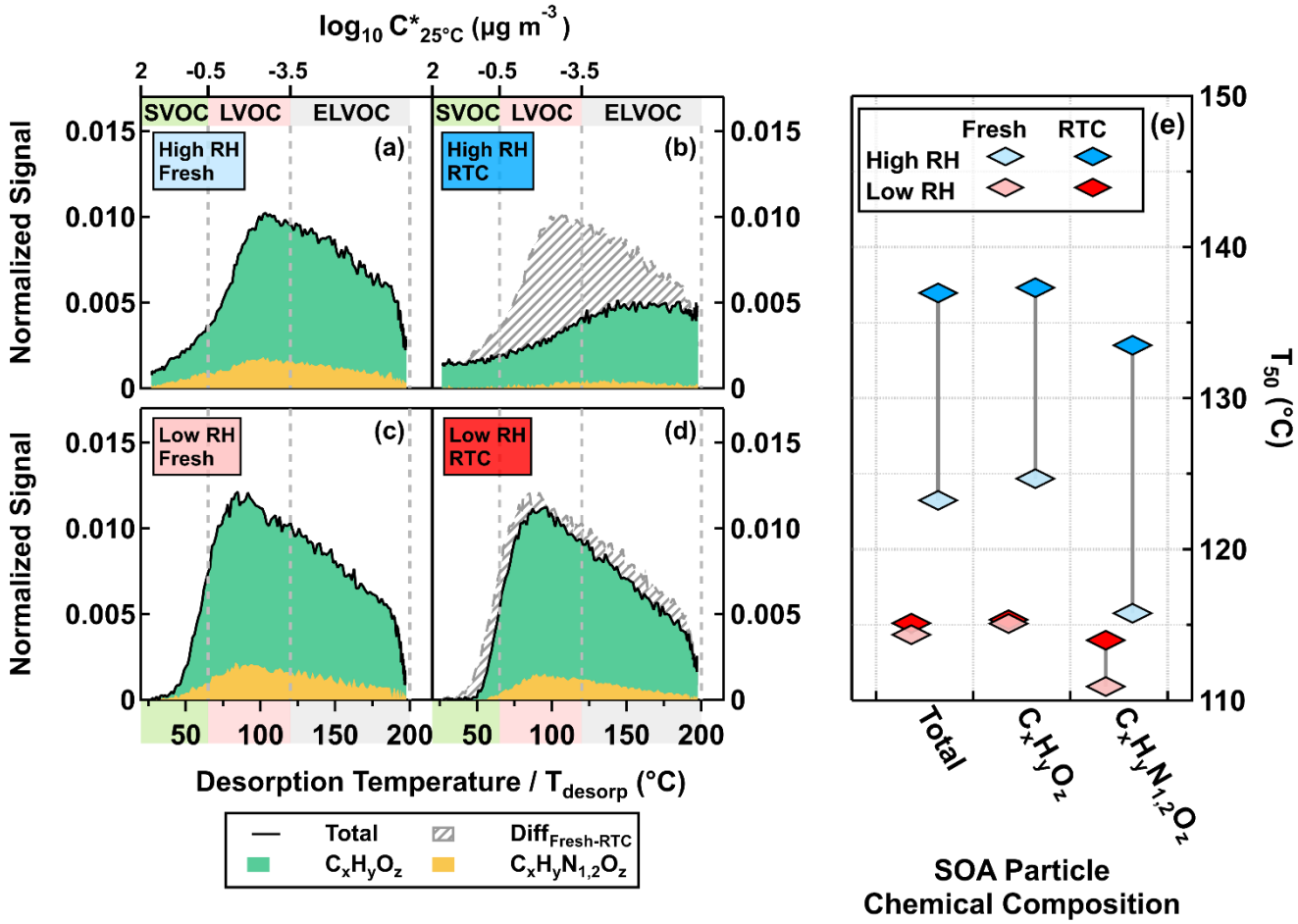
log10 C*25°C (μg m-3)
2 -0.5 -3.5
SVOC LVOC ELVOC
High RH Fresh
(a)
High RH RTC
(b)
Low RH Fresh
(c)
Low RH RTC
(d)
Normalized Signal
0.015
0.010
0.005
0
50 100 150 200
Desorption Temperature / Tdesorp (°C)
Total
CxHyOz
Diff Fresh-RTC
CxHyN1,2Oz
Fresh
RTC
High RH
Low RH
(e)
T50 (°C)
150
140
130
120
110
Total
CxHyOz
CxHyN1,2Oz
SOA Particle
Chemical Composition

855

Figure 22. FIGAERO-CIMS sum~~Sum~~ thermograms (STG) (a – d) plotted against desorption temperature (T_{desorp}) and the corresponding median desorption temperature (T_{50}, diamonds) (e) for the high-NO_x case under ~~dry~~ low RH (RH < 7 %) and high RH (80 % RH) conditions. ~~Non-nitrated organics~~CHO compounds and ~~organic nitrates~~ON are indicated by $C_xH_yO_z$ and $C_xH_yN_{1,2}O_z$, respectively. On the panels (a – d), the solid black lines indicate the total signals of STGs with the green and yellow areas marking the contributions of $C_xH_yO_z$ and $C_xH_yN_{1,2}O_z$ to the STGs, respectively., The gray-striped areas represent the differences in STGs between fresh and RTC stages. The color bands on the abscissa indicate volatility classes. Note that we presented the STGs of RTC stages after accounting for changes in the average VFR (VFR_{avg}) between fresh and RTC stages during the FIGAERO sample time.

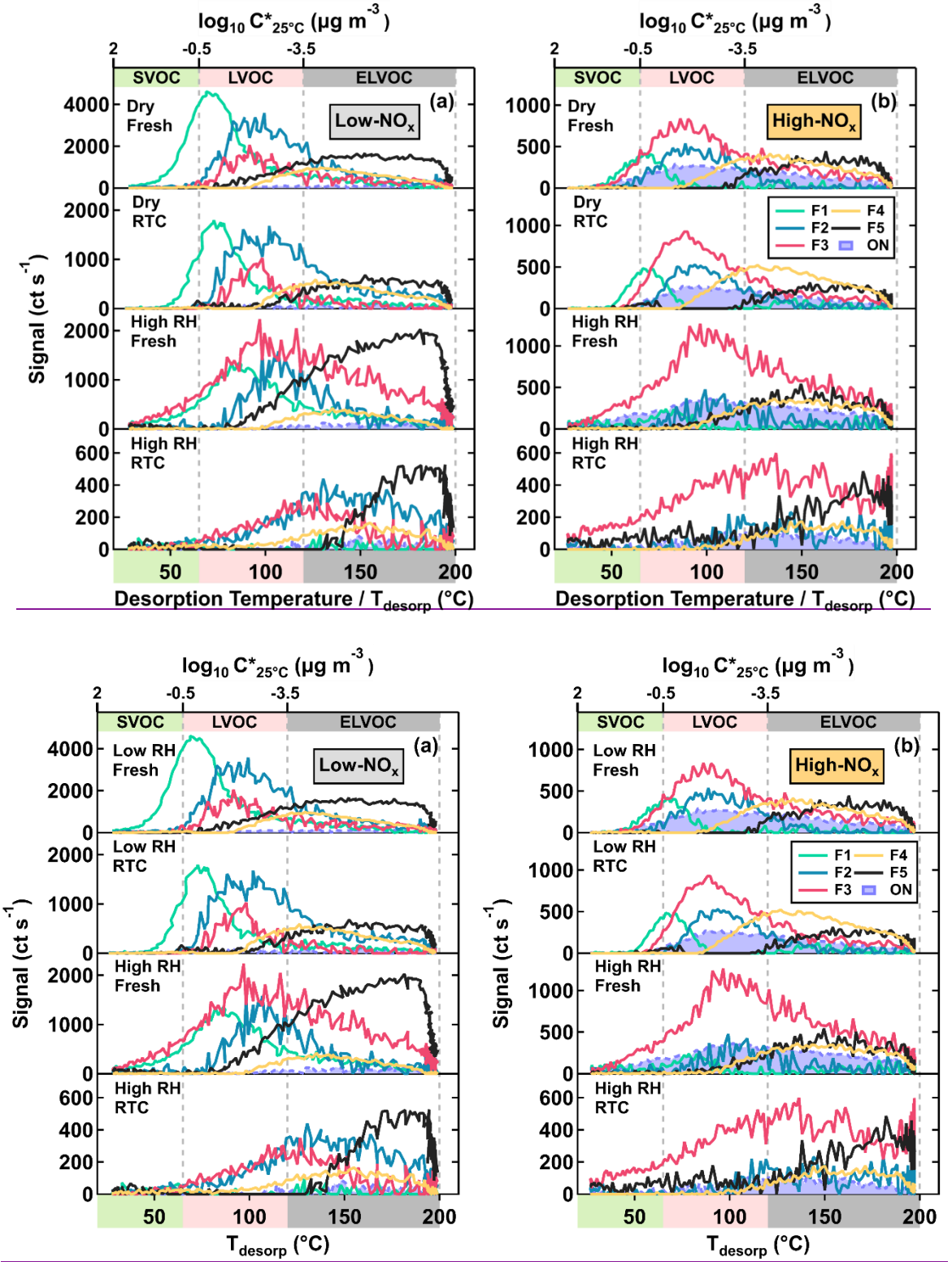

Figure 3. Factor thermograms of the five sample factors from the 12-factor PMF solution of CHO compounds in α-pinene SOA particles that were formed under low-NO_x (a) and high-NO_x (b) conditions in the OFR. In addition, thermograms of the sum of ON (sum of NF1 – 3) are shown as purple areas in panel (b). In both panels, the ranges of different volatility classes are highlighted as color bands on the abscissa.

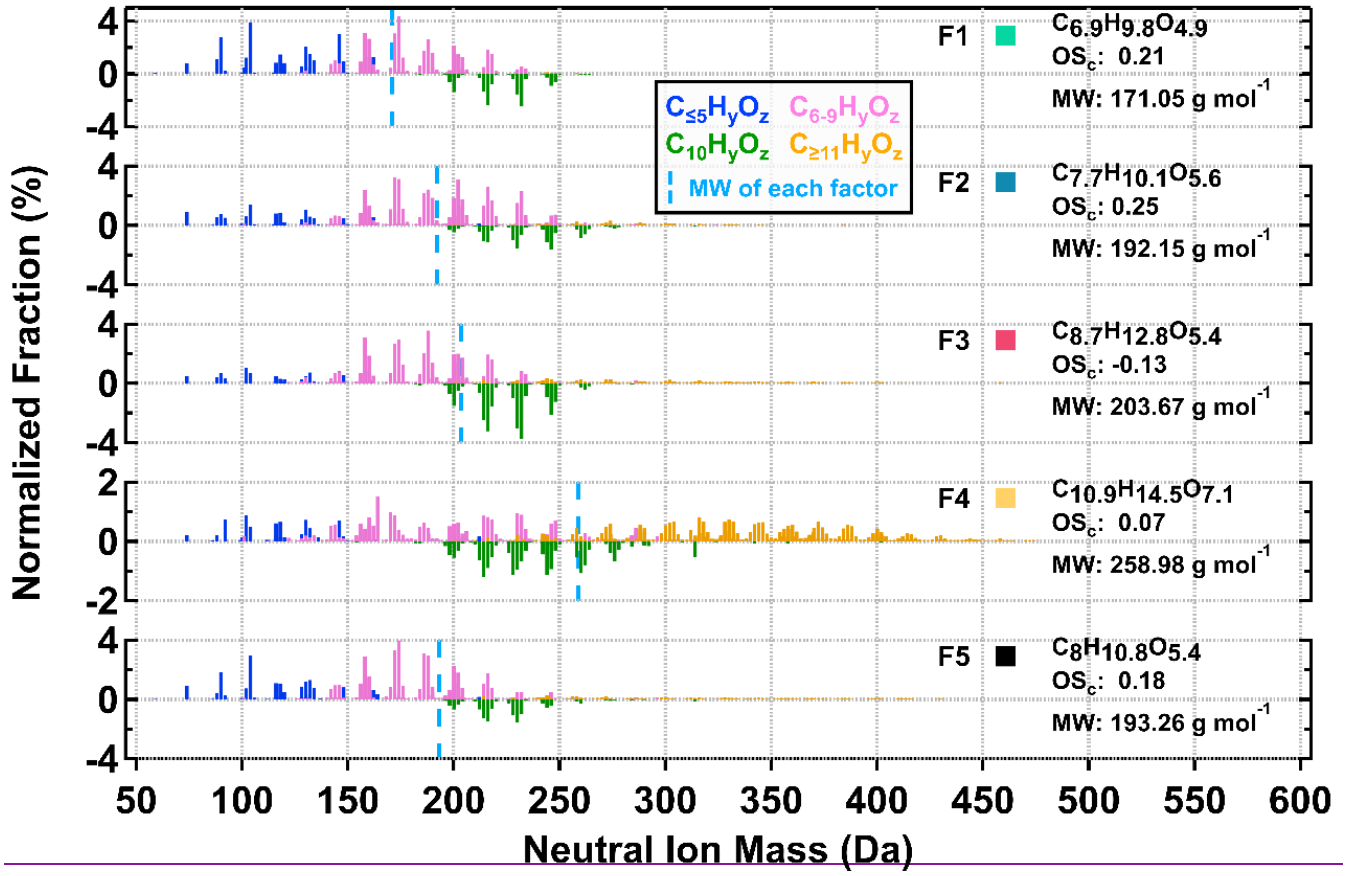

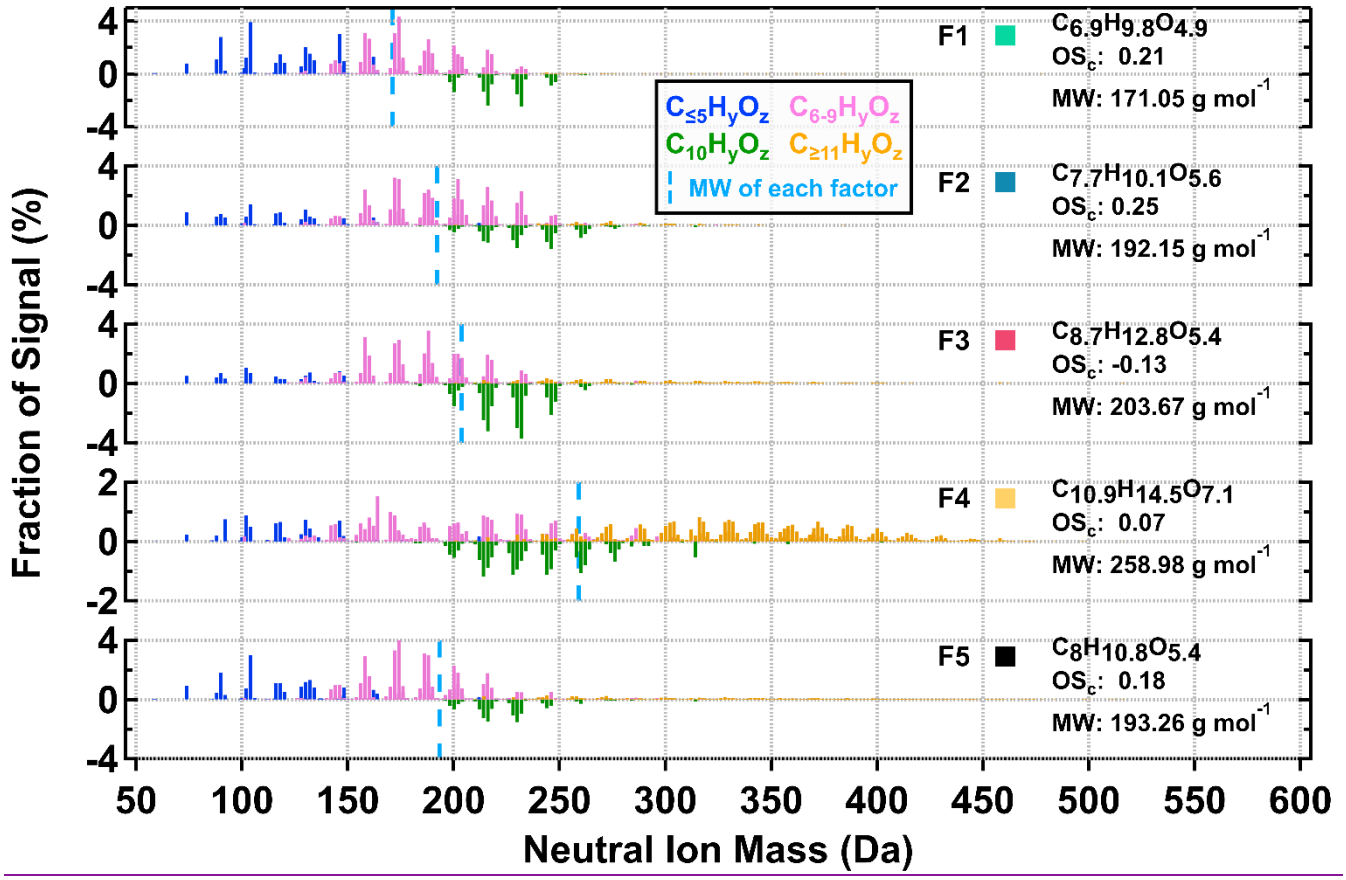

Figure 4. Normalized factor mass spectra of the five sample factors from the 12-factor PMF solution of ~~non-nitrated organics~~CHO compounds in α-pinene SOA particles that were formed under two NO_x conditions in the OFR. For readability,

$C_{10}H_yO_z$ ions are shown as negative values. For each factor mass spectrum, its signal-weighted molecular composition, molecular weight (MW), and oxidation state (OS_c) are shown on the right. Right next to each factor label, the squares are shown in the same color scheme as the factor thermograms in Figure 3 to indicate different sample factors. The blue dashed line indicates the average MW of each factor.

880

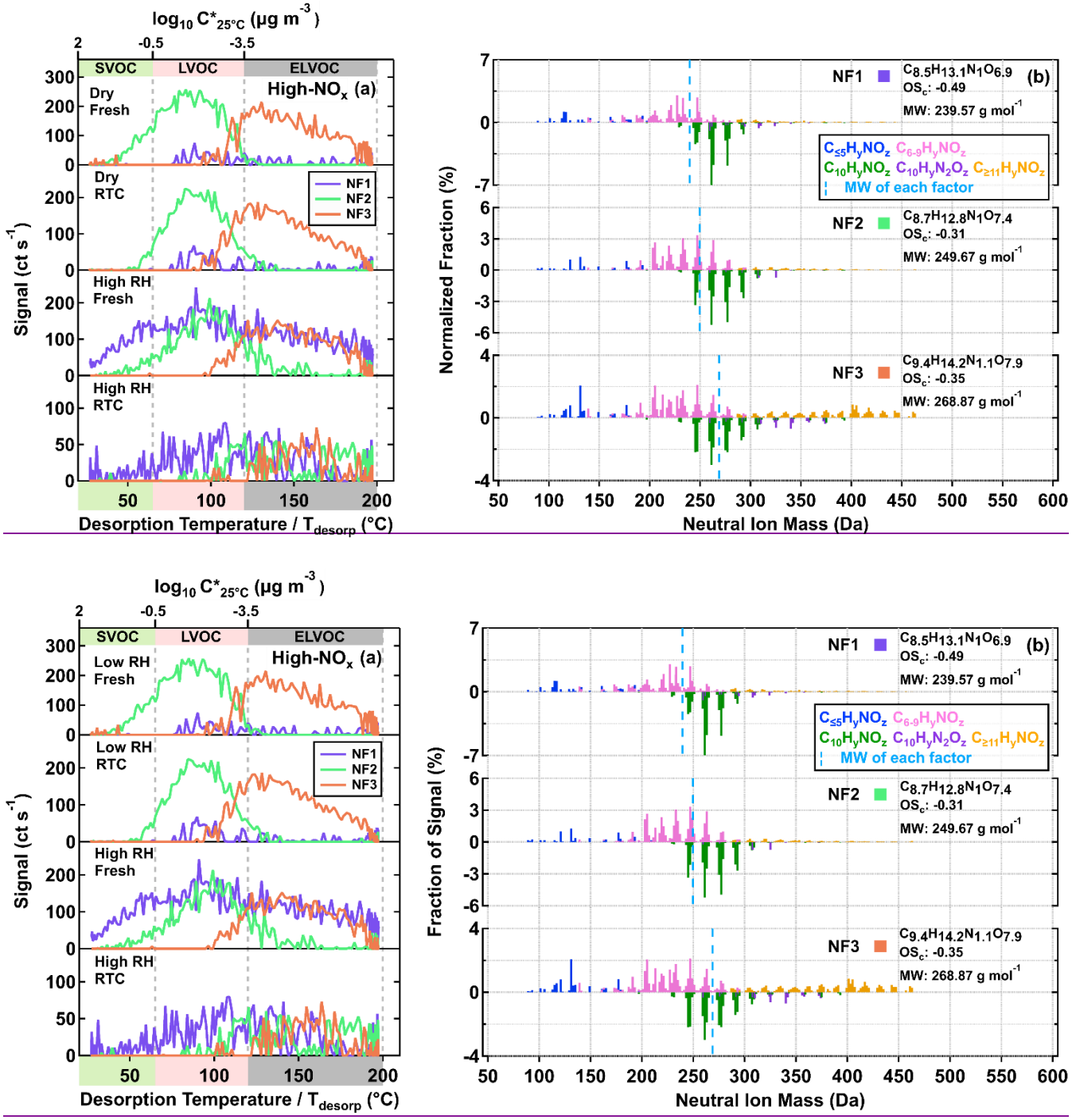

Figure 5~~5~~. Factor thermograms (a) and normalized mass spectra (b) for the three sample factors from the eight-factor solution of ~~organic nitrates~~ ON in the α-pinene SOA particles that were formed under high-NO_x conditions in the OFR. In panel (a), the ranges of different volatility classes are indicated in color bands on the abscissa. In panel (b), the bottom portion of each mass spectra represents $C_{10}H_yNO_z$. The~~the~~ signal-weighted molecular composition, molecular weight (MW), and oxidation state (OS_c) for each factor are shown on the right. Right next to each factor label in panel (b), the squares are shown in the same color scheme as the factor thermograms in panel (a) to identify different sample factors. The blue dashed line indicates the average MW of each factor.

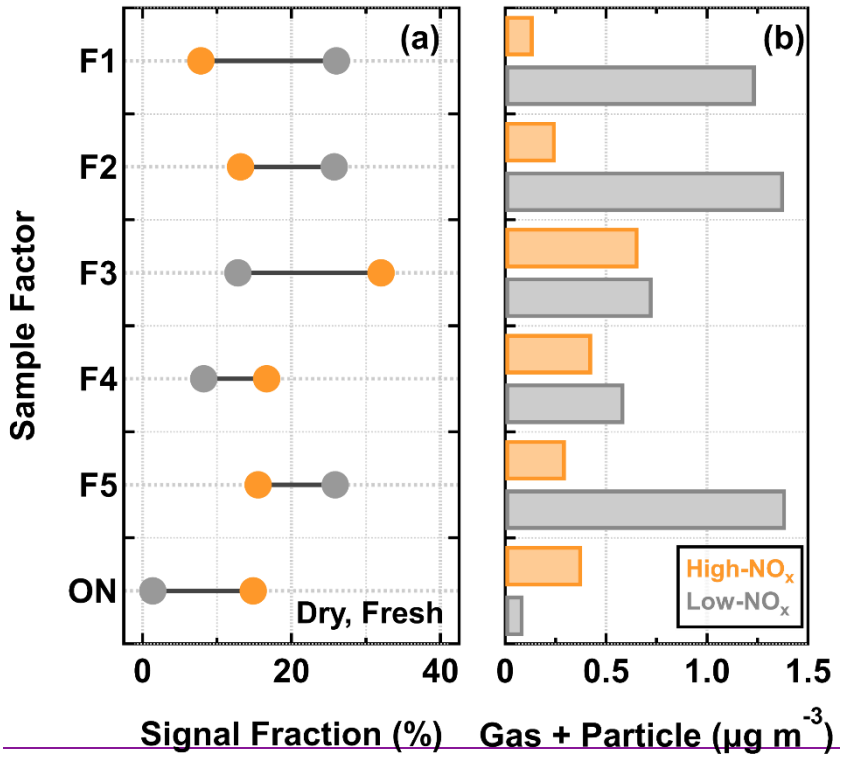

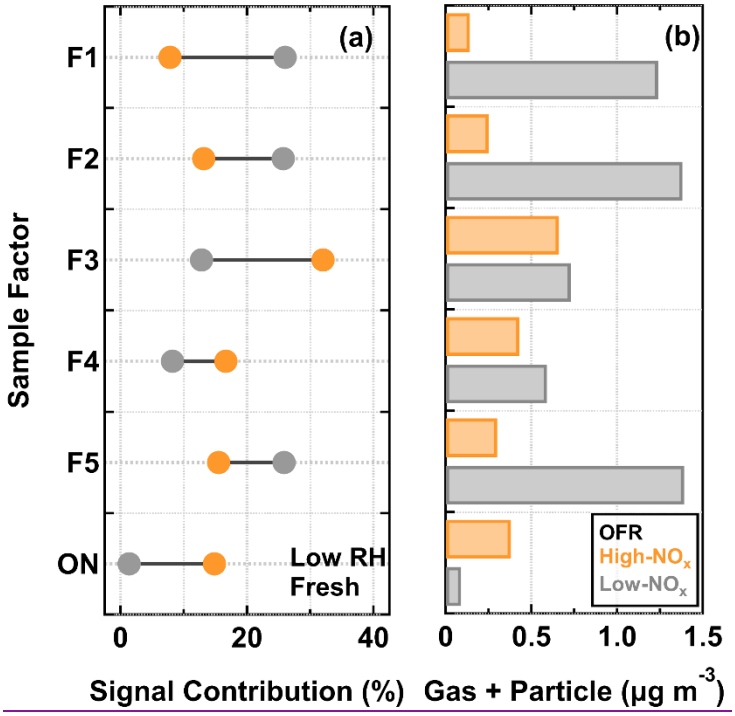

Figure 6~~6~~. Signal contributions of sample factors to their total sum (a) and the corresponding estimated mass concentrations in gas and particle phase (b) for ~~dry, fresh~~ α-pinene SOA particles that were formed under low-NO_x and high-NO_x conditions in the OFR and evaporated under low-RH and fresh condition. Note that here ON indicates the sum of the ~~organic nitrate~~ ON sample factors. The fraction is calculated by normalizing the measured sum from a PMF sample factor to the total sum of sample factors in the ~~dry~~low-RH, fresh samples under low-NO_x and high-NO_x conditions.

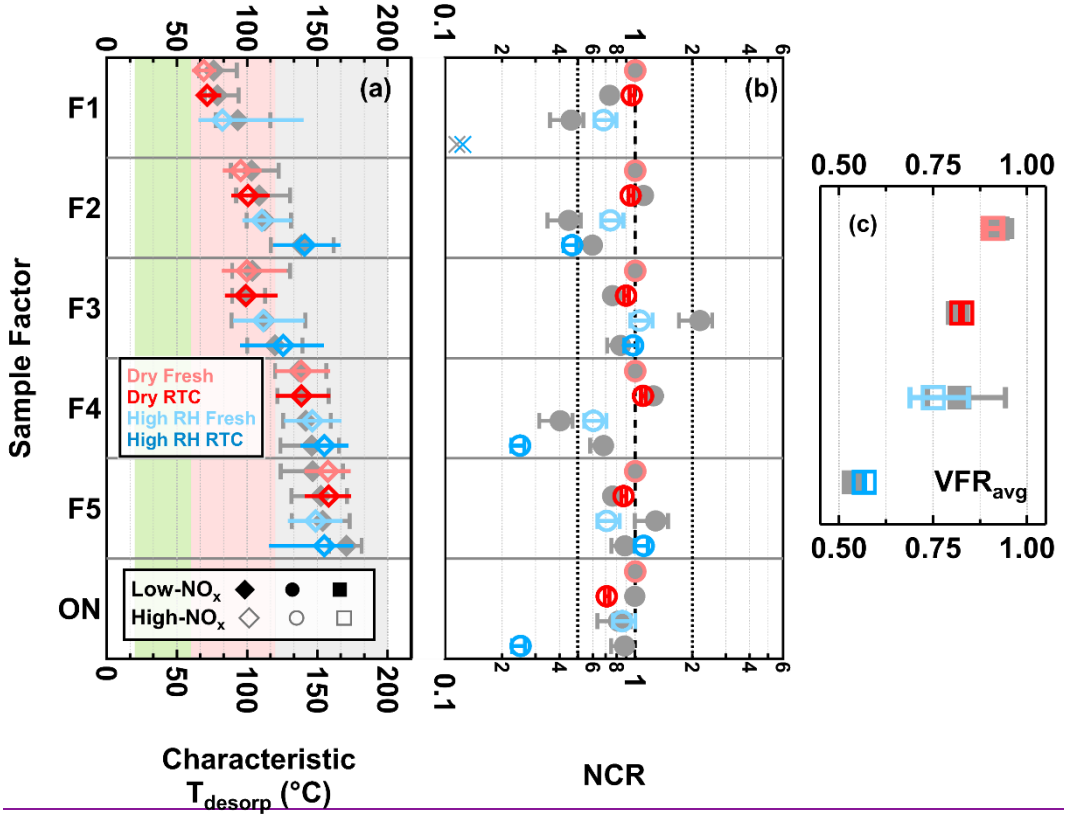
(a)
(b)
(c)
F1
F2
F3
F4
F5
ON
Sample Factor
Dry Fresh
Dry RTC
High RH Fresh
High RH RTC
Low-NOx
High-NOx
VFRavg
Characteristic Tdesorp (°C)
NCR

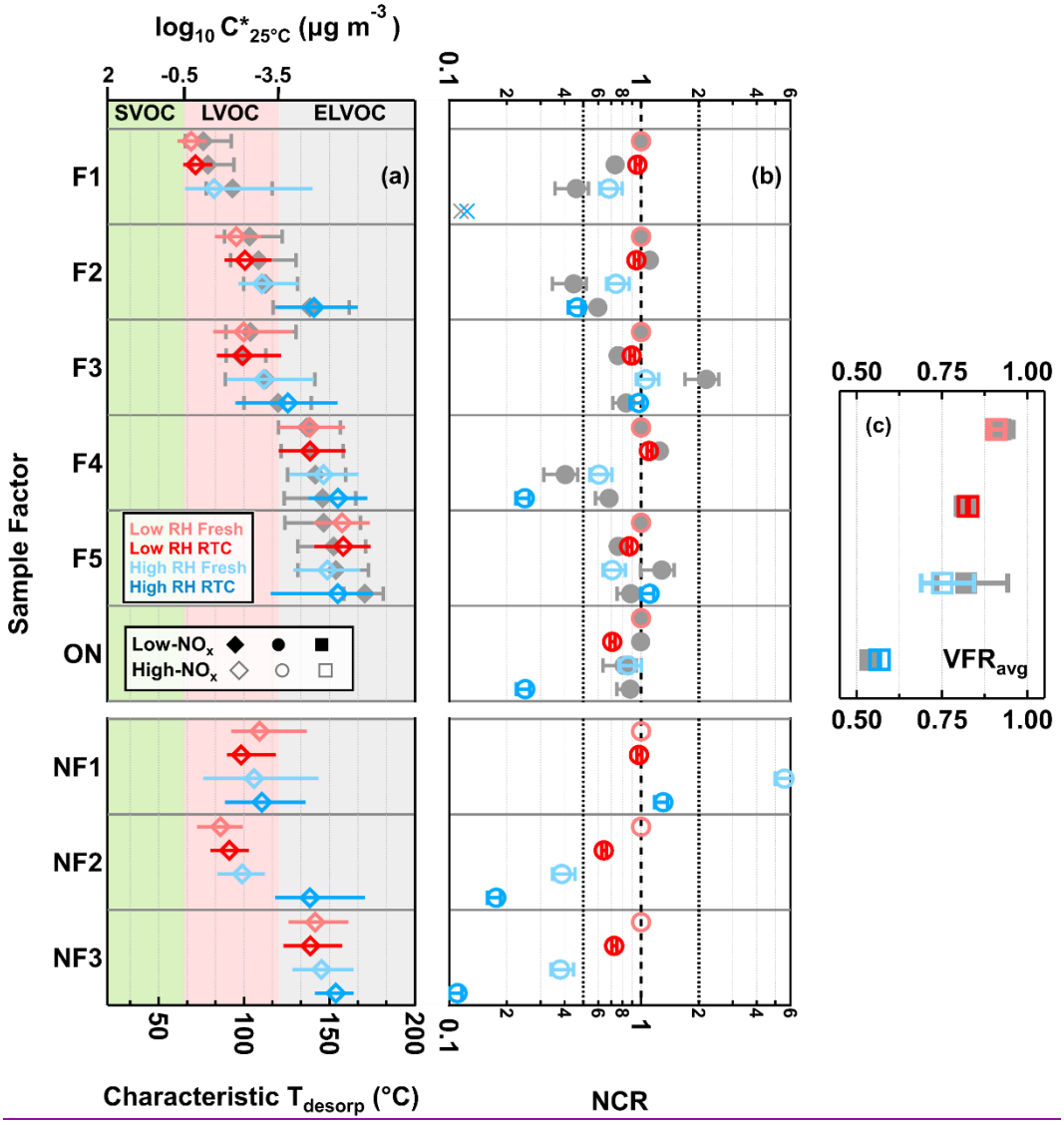
log10 C*25°C (μg m-3)
SVOC
LVOC
ELVOC
(a)
(b)
(c)
F1
F2
F3
F4
F5
ON
NF1
NF2
NF3
Sample Factor
Low RH Fresh
Low RH RTC
High RH Fresh
High RH RTC
Low-NOx
High-NOx
VFRavg
Characteristic Tdesorp (°C)
NCR

Figure 7~~7~~. Volatility and changes in factor contribution for the five ~~non-nitrated organics~~CHO and three ON sample factors and total ~~organic nitrates~~ON (~~ON,~~ sum of ~~organic nitrate~~ON sample factors). Panel (a): Characteristic desorption temperature (characteristic T_{desorp}). The marker indicates the T_{50} values, and the horizontal lines mark the interquartile range of the factor thermograms. Panel (b): Net change ratio (NCR) with error bars indicating the uncertainty stemming from the estimated range in molecular weight and particle density. Panel (c): average volume fraction remaining during sample collection (VFR_{avg}) with error bars indicating the minimum and maximum values. In all panels, the values for the high-NO_x case are shown with colored markers while the low-NO_x ones are displayed in grey. The colors indicate the sample type. The order of samples is identical for the low-NO_x and high-NO_x data. In panel (a), the range of volatility classes are highlighted with background colors ~~(green – SVOCs; red – LVOCs; grey – ELVOCs)~~. In panel (b), the dashed line at NCR equal to 1 indicates that any loss is counterbalanced by production, or no change occurs. The two dotted lines at NCR equal to 0.5 and 2 represent significant net loss and production. For F1, its factor thermogram contributes less than 5% to the total sample signal and does not show a clear maximum under the high-RH, RTC condition. Therefore, its characteristic T_{desorp} value was not estimated in panel (a) and its NCR was be indicated by a cross close to the 0.1 in panel (b).

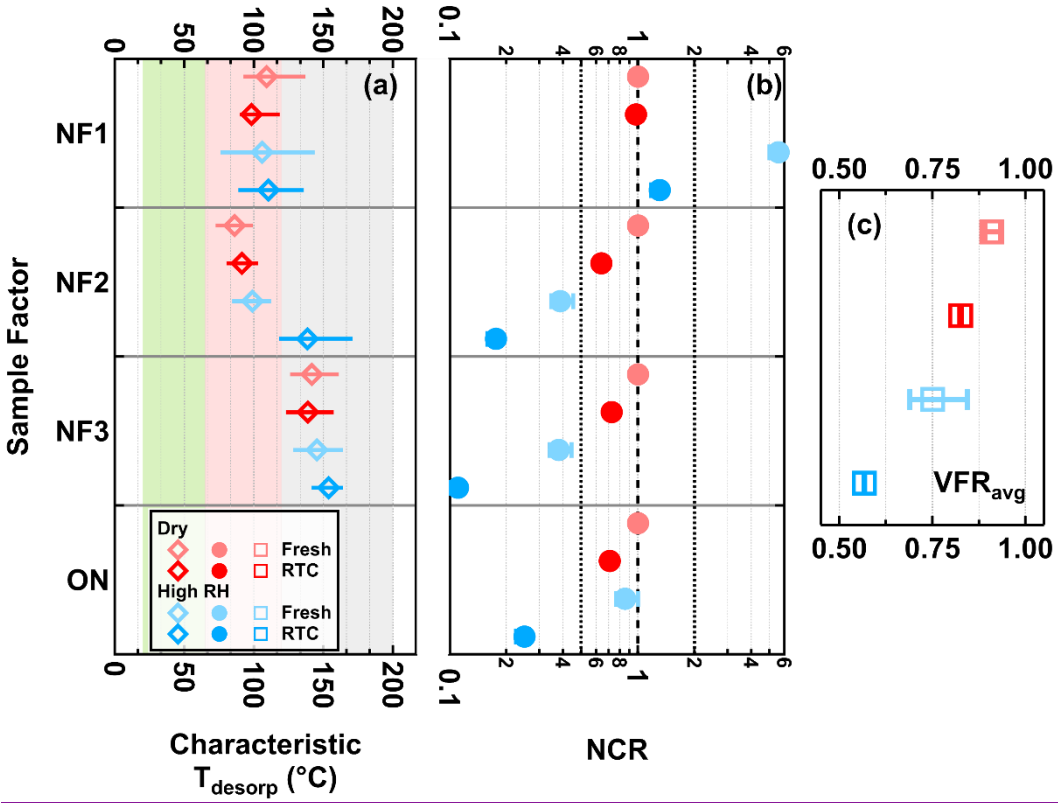

~~**Figure 8**. Volatility and changes in factor contribution for the three organic nitrate sample factors and total organic nitrates (ON, sum of organic nitrate sample factors). Panel (a): Characteristic desorption temperature (characteristic T_{desorp}). The marker indicates the T_{50} values, and the horizontal lines mark the interquartile range of the factor thermograms. Panel (b): Net change ratio (NCR) with error bars indicating the uncertainty stemming from the estimated range in molecular weight and particle density. Panel c): average volume fraction remaining during sample collection (VFR_{avg}) with error bars indicating the minimum and maximum values. The colors indicate the sample type. In panel (a), the range of volatility classes are highlighted with background colors (green – SVOCs; red – LVOCs; grey – ELVOCs). In panel (b), the dashed line at NCR equal to 1 indicates that any loss is counterbalanced by production, or no change occurs. The two dotted lines at NCR equal to 0.5 and 2 represent significant net loss and production.~~